

1     **Recent Progress for Hydrogen Production from Ammonia and Hydrous Hydrazine**  
2                     **Decomposition: A Review on Heterogeneous Catalysts**

3     Panayiota Adamou<sup>1</sup>, Silvio Bellomi<sup>2</sup>, Sanaa Hafeez<sup>3</sup>, Eleana Harkou<sup>1</sup>, S.M. Al-Salem<sup>4</sup>, Alberto Villa<sup>2</sup>,  
4                     Nikolaos Dimitratos<sup>5</sup>, George Manos<sup>3</sup> and Achilleas Constantinou<sup>1\*</sup>

- 5             1. Department of Chemical Engineering Cyprus University of Technology, 57 Corner of Athinon  
6                     and Anexartisias, 3036 Limassol, Cyprus  
7             2. Dipartimento di Chimica, Università degli Studi di Milano, via Golgi, 20133 Milan, Italy.  
8             3. Department of Chemical Engineering, University College London, London WC1E 7JE, UK.  
9             4. Environment & Life Sciences Research Centre, Kuwait Institute for Scientific Research, P.O.  
10                     Box: 24885, Safat 13109, Kuwait.  
11             5. Dipartimento di Chimica Industriale e dei Materiali, ALMA MATER STUDIORUM  
12                     Università di Bologna, Viale Risorgimento 4, 40136 Bologna, Italy.

13             \* Author for correspondence: a.konstantinou@cut.ac.cy;

14  
15     **Abstract**

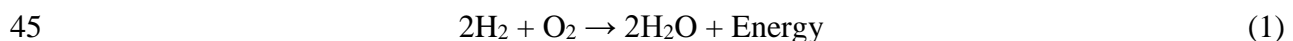
16     In response to the growing trend of greenhouse gas emissions from the production and use of  
17     conventional fuels, CO<sub>x</sub> free hydrogen generation is introduced as an alternative and efficient  
18     energy carrier. Due to hydrogen's storage challenges, is more efficient to be produced *on-site*  
19     by other chemical compounds for fuel cell applications. This work outlines the production of  
20     hydrogen (H<sub>2</sub>) from ammonia (NH<sub>3</sub>) and hydrous hydrazine (N<sub>2</sub>H<sub>4</sub>.H<sub>2</sub>O) catalytic  
21     decomposition. Both of these substances are giving nitrogen (N<sub>2</sub>) as a by-product, which is not  
22     toxic. Moreover, heterogeneous catalysts that were studied through the years are presented.  
23     Lastly, a reactoristic view of the ammonia decomposition is provided with different reactors  
24     such as catalytic membrane reactors (CMRs), fixed-bed reactors (FBRs) and micro-reactors  
25     (MRs) for the evaluation of their performance.

26     Keywords: Ammonia, Hydrous Hydrazine, Hydrogen, Catalysts, Reactors

## 30 1 Introduction

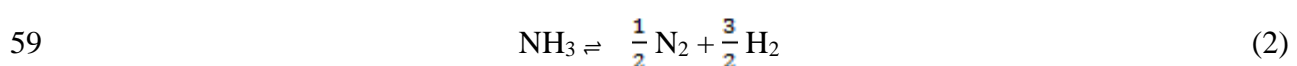
31 Environmental concerns are increasing as the extensive use of fossil fuels in the energy sector  
32 is the biggest contributor to climate change. Fossil fuels undergo the process of combustion to  
33 release their energy content, polluting the atmosphere with emissions of greenhouse gases  
34 (GHGs) and harmful substances. These resources are non-renewable and are not evenly  
35 distributed around the world [1]. There is an increasing urge in recent years to find and adopt  
36 alternative emission-free energy sources in hope to stabilise the negative impacts conventional  
37 fuels have created in the environment. Hydrogen (H<sub>2</sub>) is preferred as an energy carrier due to  
38 its zero emissions during combustion and its generation from various paths such as non-  
39 renewable sources, biomass and water electrolysis [2].

40 Hydrogen can be produced by either from fossil fuels, capturing carbon emissions or renewable  
41 resources. Depending on the material, H<sub>2</sub> can be classified as grey, blue, and green respectively.  
42 Two of the common methods to produce H<sub>2</sub> is steam methane reforming and water splitting  
43 reactions such as water electrolysis [3–6]. Fuel cells then can be used to convert H<sub>2</sub> into power  
44 through the electrochemical reaction that follows (Eq. 1):



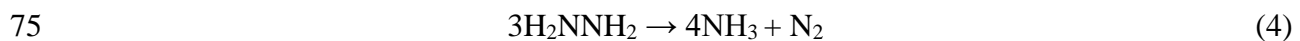
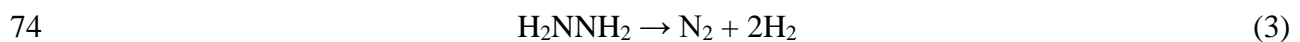
46 Eq. 1 shows H<sub>2</sub> reaction with oxygen to produce water and energy in the form of electricity or  
47 heat as the inverse reaction of electrolysis. Fuel cells are very promising and are already used  
48 in various stationary and mobile applications such as back-up power supplies, road vehicles,  
49 as well as rockets and space shuttles. The main concept revolves around generating green  
50 energy which is considered revolutionary [7]. However, its storage and transportation problems  
51 have not yet reached an applicable level for further industrial use.

52 Ammonia (NH<sub>3</sub>), among other H<sub>2</sub> energy sources, is a promising alternative. It is mainly  
53 produced from the decomposition of urea and other nitrogen compounds during wastewater  
54 treatment processes or from the microbial decomposition of organic substances containing  
55 nitrogen [8]. It possesses high H<sub>2</sub> content (17.8 wt%) and a large energy density (3000 Wh/kg).  
56 It has greater volumetric hydrogen density than liquid H<sub>2</sub> (121 kg H<sub>2</sub>/m<sup>3</sup>) and can be liquefied  
57 and stored at room temperature facilitating transportation and storage [9–12]. Furthermore, the  
58 decomposition of ammonia is CO<sub>x</sub>-free producing only H<sub>2</sub> and nitrogen (N<sub>2</sub>) (Eq. 2) [13].



60 Ramsay and Young [14] were the first to study the temperature at which ammonia  
61 decomposition takes place and the influence of the vessel or tube material that contains the gas  
62 in the early 1880s. Then at the beginning of the 20<sup>th</sup> century Perman and Atkinson [15] studied  
63 both the effect of temperature and pressure on the rate of decomposition as well as the catalytic  
64 activity of Hg, Fe, and Pt.

65 Hydrous hydrazine (N<sub>2</sub>H<sub>4</sub>·H<sub>2</sub>O) has also been proposed as a promising candidate for H<sub>2</sub>  
66 generation. It can be produced by the Raschig process that involves the ammonolysis of  
67 hypochlorite to hydrazine and ammonia or the oxidation of anhydrous ammonia by chlorine  
68 [16]. Hydrous hydrazine has a high hydrogen content (8.0 wt%) and due to its carbon-free  
69 content, the generation of H<sub>2</sub> has zero emissions [17]–[20]. The products from hydrazine  
70 decomposition are H<sub>2</sub> and N<sub>2</sub>; however, an undesirable side reaction of incomplete  
71 decomposition may occur producing ammonia, which must be avoided because it reduces the  
72 efficiency of the H<sub>2</sub> generation process. The two reaction pathways for hydrazine  
73 decomposition are depicted in Eqs. (3-4) [21].



76 This review will highlight H<sub>2</sub> storage challenges and the generation of H<sub>2</sub> from ammonia and  
77 hydrous hydrazine. Moreover, the heterogeneous catalysts for the decomposition of the  
78 substances mentioned above and the structural properties of the catalysts, will be addressed.  
79 Furthermore, different types of reactors that have been applied for the ammonia decomposition,  
80 will be covered to provide an overview of the most innovative and efficient future systems.  
81 Regarding hydrous hydrazine, there are not many studies in reactors and therefore, reactor set-  
82 ups will be not discussed.

83

## 84 **2 Hydrogen Storage Challenges**

85 Although H<sub>2</sub> offers an attractive and promising solution as an alternative energy carrier, its  
86 storage and transportation are one of the main technical barriers preventing H<sub>2</sub> for wider  
87 applications. This is due to hydrogen's very low density of 0.089 kg/m<sup>3</sup> at 0°C and 1 bar. At  
88 ambient temperatures and 1 atm pressure, 1 kg of H<sub>2</sub> occupies 11 m<sup>3</sup>, which results in a large  
89 volume required for storage. Nonetheless, H<sub>2</sub> is extremely flammable with a flame speed nearly

90 an order of magnitude higher than gasoline when mixed with air, therefore, its safety issues  
91 must be resolved [22].

92 Due to the lack of appropriate infrastructure for storage, transportation and distribution of H<sub>2</sub>,  
93 new methods must be found to store it safely. For large scale and long-term storage, different  
94 underground storage sites were proposed such as salt caverns, aquifer formations or depleted  
95 oil and gas fields. Salt caverns are currently the most favorable method. No in-situ reactions  
96 either with microorganisms or any chemical elements occurred so far and the leakage rates are  
97 very low because salt caverns exhibit the required tightness. In contrast with aquifer formations  
98 or depleted oil and gas fields that occur naturally, salt caverns need to be developed in an  
99 already existing underground salt formations, so not all regions have the necessary geological  
100 characteristics [23].

101 Moreover, it is necessary to increase the volumetric energy (density) of H<sub>2</sub> which can happen  
102 either by liquefying it or by compressing it. Pressurised tanks can take the form of cylindrical  
103 or spherical vessels or bottles, and while raising the pressure, gaseous H<sub>2</sub> density increases  
104 achieving higher storage density. These are currently used in stationary applications mainly to  
105 store hydrogen in hydrogen refuelling stations [24]. Their cost may differ from the material  
106 used and the pressure applied in the tank. On the other hand, cryogenic tanks store liquefied  
107 hydrogen at -253°C (atmospheric pressure) because the liquefaction process increases H<sub>2</sub>  
108 volumetric density drastically. These are not designed to withstand high pressures inside, hence  
109 they must be isolated to reduce as much as possible heat transfer. However, compressing  
110 requires high pressures and liquefying needs extremely low temperatures such as -253°C that  
111 can only be achieved with multiple heat exchangers and a combination of multiple cooling  
112 cycles [25].

113 New technologies such as metal hydrides and carbon nanotubes are gaining attention for their  
114 H<sub>2</sub> storage properties. Metal hydrides can store H<sub>2</sub> due to their large storage capacity at ambient  
115 pressure and temperature. Hydrogen reacts with metals which have the ability to absorb and  
116 desorb it by breaking or bonding the chemical bonds making them an efficient form of  
117 hydrogen storage [26]. Adsorption of H<sub>2</sub> in carbon nanostructures is an attractive solution for  
118 hydrogen storage due to the high surface area of carbon. There are a variety of carbon materials,  
119 such as single walled carbon nanotubes (SWCNTs), multiwalled carbon nanotubes (MWCNTs)  
120 and carbon nanofibers (CNFs). However due to some controversial results that were obtained  
121 from some studies regarding the H<sub>2</sub> adsorption measurements, much research is still needed for

122 their efficient usage [27]. For example, in the late 1990s, Dillon et al. [28] suggested that  
123 SWCNTs have a very high H<sub>2</sub> uptake up to 5-10%. Moreover, Chambers et al. [29] published  
124 an even more extraordinary result. It was claimed that the hydrogen storage capacity of graphite  
125 nanofibers (GNFs) materials was up to 67.55 %. Both of these results were questionable thus  
126 research groups [30]–[32] tried to reproduce and validate the results without success since the  
127 capacity of the materials was very much lower.

128

### 129 **3 Hydrogen Production Routes**

130 Various raw materials can be utilised to produce H<sub>2</sub> following different production routes.  
131 Given the raw material, H<sub>2</sub> can be colour coded as black, grey, blue or green.

132 In spite of the growing number of studies focusing on renewable hydrogen production, fossil  
133 fuel-based hydrogen generation is still being examined. Black or brown H<sub>2</sub> is produced from  
134 coal through the process of gasification. It is considered a very environmentally damaging  
135 method as carbon dioxide and carbon monoxide are also generated and emitted in the  
136 atmosphere. Liu et al. [33] investigated the gasification mechanism and developed a coal  
137 supercritical water gasification reaction kinetic model taking into consideration the migration  
138 mechanism of nitrogen and sulfur. The model could not only predict the generation of  
139 hydrogen, carbon monoxide and carbon dioxide but ammonia and hydrogen sulfide as well,  
140 proving the interaction between hydrocarbon gas and the gasification products of nitrogen and  
141 sulfur.

142 H<sub>2</sub> is labelled grey when extracted from natural gas via steam-methane reforming. It is the most  
143 common form nowadays with over 95% of the global hydrogen production coming from  
144 reforming of conventional fuels and around 50% of that is generated from steam reforming of  
145 natural gas [4]. SMR is an endothermic reaction (600-700°C) and the catalysts mostly used for  
146 this reaction are nickel-based. Ngo et al. [34] utilised a SMR unit with a furnace and a reactor,  
147 where the furnace produces heat via the natural gas reaction with oxygen and the reactor  
148 consumes heat and generates H<sub>2</sub>. Another study conducted by Cho et al. [35] used facility-level  
149 data to examine the pollutant emissions which may differ from the theoretical estimates due to  
150 various process conditions and types of pollution controlled equipment. Direct emissions from  
151 the 33 facilities used were 9.35 kg CO<sub>2</sub>/kg H<sub>2</sub> and increased up to 11.2 kg CO<sub>2</sub>/kg H<sub>2</sub> when the

152 full cycle of H<sub>2</sub> production was included. Increasing 10% in hydrogen production efficiency  
153 the global warming impact can be reduced up to 11.1%.

154 Blue H<sub>2</sub> is produced from fossil fuels like black and grey H<sub>2</sub> but the carbon generated from the  
155 process is captured. It can be described with the term carbon neutral but low-carbon H<sub>2</sub> would  
156 be a more appropriate term since not all carbon emissions are captured. Even though CO<sub>2</sub> can  
157 be captured by absorbents or amine solvents, it must be stored after, which is costly. Therefore  
158 Khan et al. [36] explored the possibility to use the carbon captured by converting into formic  
159 acid by the electroreduction. An amine-based CO<sub>2</sub> capture unit was utilised with 90% capture  
160 efficiency. The carbon could either be stored or utilised. It was concluded that by utilising it  
161 instead of storing it, is more cost-effective and is a promising approach for further future work.

162 Lastly, green H<sub>2</sub> uses renewable sources such as biomass, geothermal, wind and solar energy  
163 [37]. One of the most common methods used to obtain green H<sub>2</sub> is water splitting reactions  
164 such as electrolysis of water. Water reacts at the cell's anode and under the influence of current  
165 it decomposes and produces O<sub>2</sub> at the anode of the cell and finally H<sub>2</sub> at the cathode [38].  
166 Another common method is the dehydrogenation of hydrogen carrier compounds with zero  
167 CO<sub>2</sub> emissions that will be discussed later.

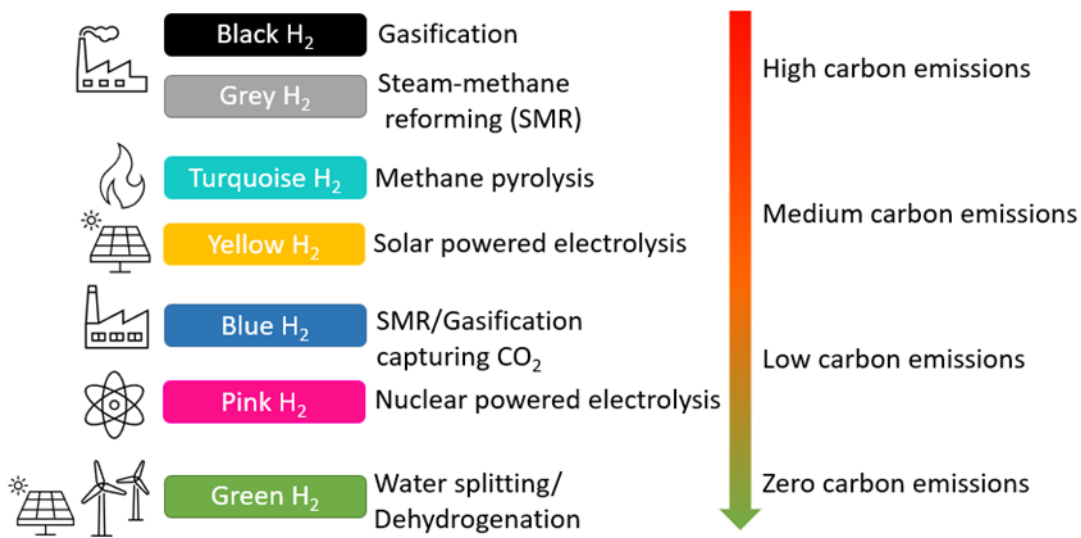
168 Apart from these, H<sub>2</sub> can be classified to turquoise, pink, yellow and white which are not  
169 commonly used. Turquoise refers to H<sub>2</sub> produced from methane pyrolysis with solid carbon as  
170 a by-product. Even though methane pyrolysis is not a sustainable process since natural gas  
171 reserves are depleting, it can provide a temporary solution until renewable technologies are  
172 fully developed. The process begins with the cracking of methane to H<sub>2</sub> and solid carbon, then  
173 the removal of the carbon from the stream and lastly, the purification of the gas stream. High  
174 temperatures are needed for methane pyrolysis, up to 1000°C for non-catalytic systems.  
175 Suitable catalysts such as nickel, iron, and carbon have been extensively studied and the  
176 decomposition of methane can be triggered at lower temperatures (500-800°C) [39].

177 Pink (or purple) and yellow H<sub>2</sub> are both produced through electrolysis using nuclear power and  
178 solar power respectively [40]. Water electrolysis technology consists of an anode, a cathode,  
179 an electrolyte, and power supply. Then, electrons flow from the direct current source's to  
180 cathode where hydrogen is formed along with oxygen. The difference from conventional  
181 electrolysis to nuclear high temperature electrolysis (HTE), is that the later uses heat from  
182 nuclear power plants to moderate electricity consumed for electrolysis. In general, nuclear HTE  
183 occurs at 800-1000°C and an yttria-stabilised zirconia is used as an electrolyte [41]. A solar-

184 based electrolysis consists of a concentrating collector, a heat engine, an electrical generator,  
 185 and electrolyser. A part of the absorbed solar radiation is converted to mechanical work and  
 186 then the electrical generator transforms it to electrical power. Then, the generated electricity is  
 187 used to electrolyse water and produce H<sub>2</sub> and O<sub>2</sub> [42].

188 White H<sub>2</sub> refers to the by-product obtained from industrial processes such as catalytic  
 189 thermochemical splitting of water, or it may be referred as its natural occurring form. The  
 190 thermochemical splitting occurs without intermediate step and is based on the use of  
 191 concentrated solar energy. This pathway may further reduce economic and environmental costs  
 192 [43].

193 Potential applications of H<sub>2</sub> after its production are its use as an industrial feedstock, power  
 194 generation, stationary and transportation [44]. Fig. 1 summarises the H<sub>2</sub> colour spectrum  
 195 according to the feedstock and production used.



196 Fig.1. Hydrogen colour spectrum.

197

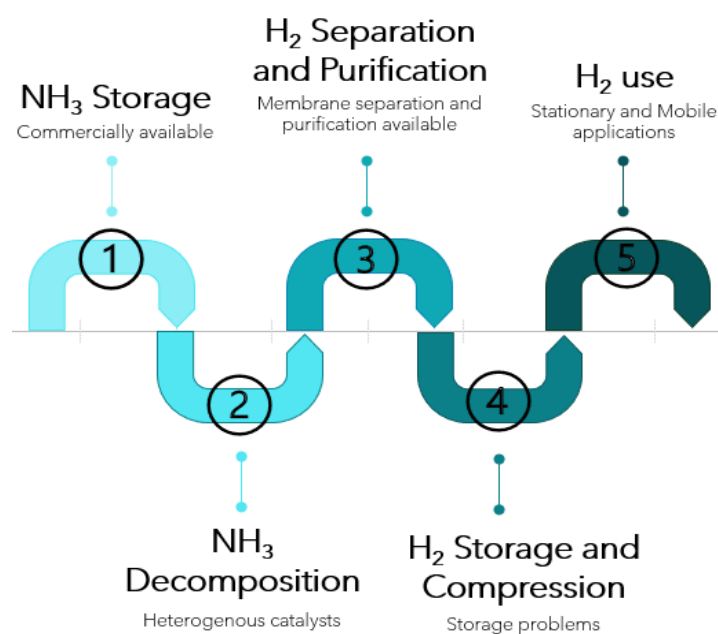
## 198 **4 Ammonia Decomposition as a sustainable hydrogen production method**

### 199 **4.1 Heterogeneous Catalysis of Ammonia**

200 Heterogeneous catalysis can be described as the catalysis whereas the phase of the catalyst is  
 201 different from the phase of the reactants/products. Thus, heterogeneous catalysts are, mostly,  
 202 in the solid state while the reactant mixture is either liquid or gas, in contrast with homogeneous

203 catalysts that exist in the same phase with the mixture. Heterogeneous catalysts have the ability  
204 to regenerate, separate easily from the products, shaped into different geometries and give high  
205 rates [45]. Table 1 summarises the most effective heterogeneous catalysts utilized for the  
206 decomposition of ammonia.

207 Since the 19<sup>th</sup> century, ammonia decomposition has been investigated mostly to understand the  
208 ammonia synthesis with the presence or absence of catalysts. Over the last decade, the catalytic  
209 decomposition of ammonia has gained a lot of attention and catalysts such as platinum (Pt)  
210 [46], palladium (Pd) [47], ruthenium (Ru) [48] and, rhodium (Rh) [49] that were known to  
211 catalyse ammonia synthesis have been used in different experiments [50]. Ru was found to be  
212 the most active and studied catalyst as there is a plethora of studies according to Ru-based  
213 catalysts [51]–[55]. Unfortunately, the large scale of application of Ru catalysts is not cost  
214 effective and their limited availability leads to the necessary development of cheaper catalytic  
215 systems with the same efficacy. The production steps of H<sub>2</sub> by ammonia are depicted in Fig.2.



216 Fig.2. Production steps of hydrogen by ammonia [12].

217 Ni metal particles were used as catalysts with MgAl<sub>2</sub>O<sub>4</sub> as supports by Qiu et al. [56] for  
218 investigation of the support effect on the catalytic decomposition of ammonia. From the  
219 catalysts tested Ni/MgAl<sub>2</sub>O<sub>4</sub> – LDH, developed by hydrothermal synthesis, had the best  
220 catalytic activity with 88.7% NH<sub>3</sub> conversion and a H<sub>2</sub> production rate of 1782.6 mmol g<sub>cat</sub><sup>-1</sup> h<sup>-1</sup>  
221 <sup>1</sup> at 600 °C with a stable performance for a period of 30 h. Ni/MgAl<sub>2</sub>O<sub>4</sub> – LDH catalyst had the  
222 highest surface area (148.3 m<sup>2</sup>/g) and therefore it resulted in high Ni dispersion (29.6 %)



223 enhancing the NH<sub>3</sub> conversion and weakening the H<sub>2</sub> poisoning. Ni/MgAl<sub>2</sub>O<sub>4</sub> – LDH catalyst  
224 was further examined for its stability at a temperature range of 550-650°C for 24 h and the  
225 results showed that the catalyst was highly stable due to the strong metal-support interactions.  
226 It was concluded that this catalyst with high stability, activity, and low cost it is essential to be  
227 developed more and used in upscale application for H<sub>2</sub> generation.

228 Cobalt particles supported on carbon doped with nitrogen were prepared via pyrolysis of ZIF-  
229 67 at a range of temperatures (Co/NC-X, X = 500, 600, 700 and 800°C) by Li et al. [57]. The  
230 synthesis process of the catalysts resulted in an evenly dispersion of the Co particles hindering  
231 their aggregation. At temperatures below 300°C the catalysts were inactive. While increasing  
232 the temperature the conversion of ammonia increased and the best catalytic activity was  
233 obtained by Co/NC-600 with an NH<sub>3</sub> conversion of 80 % and H<sub>2</sub> production rate of 26.78 mmol  
234 H<sub>2</sub> g<sub>cat</sub><sup>-1</sup> min<sup>-1</sup> at 500°C and hardly decreased even after 72 h. The bond strength between the  
235 metal and nitrogen, according to previous studies, plays a key role in the decomposition of  
236 ammonia. If the bond is either too weak or too strong it affects the adsorption of NH<sub>3</sub> and the  
237 desorption of the intermediate products resulting in a low catalytic activity. Thus, medium  
238 metal-nitrogen bond strength is required for this reaction and from further investigation it was  
239 found that the Co-N bond energy of Co/NC-600 catalyst is in the middle range and thus acting  
240 beneficial for the reaction.

241 Ru particles supported on SmCeO<sub>x</sub> were investigated by Tang et al. [58] for evaluation of the  
242 effect of the Sm doping to the catalysts. At 400°C, the Ru/SmCeO<sub>x</sub> catalyst, with 1.4 nm  
243 average particle size, obtained a conversion rate of 74.9 % corresponding to a H<sub>2</sub> production  
244 rate of 161.1 mmol g<sub>Ru</sub><sup>-1</sup> min<sup>-1</sup>, much higher than other supports with Ru particles tested for  
245 this catalytic reaction. Characterization techniques were used to study the properties and  
246 structure of the Ru/SmCeO<sub>x</sub> catalyst. The high activity was attributed to the doping of Sm that  
247 formed in plenty of oxygen vacancies which have strong interaction with Ru resulting in a high  
248 Ru dispersion.

249 A series of Co<sub>3</sub>O<sub>4</sub> catalysts supported on barium hexaaluminate (BHA) with various mass  
250 loadings of Co (XCo/BHA, X = 10%, 20%, 30%, 35% and 40%) and 0.5 g BHA were prepared  
251 by Li et al. [59]. BHA alone was inactive and with an increase of Co loading the activity also  
252 increased. The 35Co/BHA catalyst demonstrated the highest catalytic activity among the others  
253 with a conversion rate of 87.2% at 500°C and a H<sub>2</sub> production rate of 29.2 mmol H<sub>2</sub> g<sub>cat</sub><sup>-1</sup> min<sup>-1</sup>  
254 <sup>1</sup>. After 200 h the conversion rate was at 85% indicating the catalysts great stability.

255 Ru-based catalysts supported on reduced graphene oxide were developed by Pinzón et al. [60]  
256 for hydrogen generation by ammonia decomposition. The effect of the Ru loading as well as  
257 the effect of the amount of the support material were examined. With a content of Ru up to 2.5  
258 wt% , an increase in the catalytic activity was noticed (92%), while Ru loading higher than 2.5  
259 wt% resulted in agglomeration decreasing the number of active sites and therefore the ammonia  
260 conversion. With the addition of the pre-reducing agent the catalytic activity increased. The  
261 optimal catalytic activity was observed from 2.5Ru/10C-rGO catalyst with a conversion of 96%  
262 and H<sub>2</sub> production rate of 349.7 mmol H<sub>2</sub> g<sub>Ru</sub><sup>-1</sup> min<sup>-1</sup>. After 60 h of reaction the catalyst did not  
263 show any significant change in its performance.

264 In an attempt to imitate the activity of the Ru catalysts, Kirste et al. [61] developed alloys of  
265 different unsupported bimetallic catalysts (CoRe<sub>1.6</sub>, Ni<sub>2</sub>Mo<sub>3</sub>N and Co<sub>3</sub>Mo<sub>3</sub>N) for the on-  
266 demand production of H<sub>2</sub> via ammonia decomposition. In parallel, 7 wt% Ru/CNTs catalytic  
267 particles were also synthesized to compare the catalytic activities. CoRe<sub>1.6</sub> obtained a similar  
268 activity with Ru/CNTs due to the alloy synergistic effect. The catalyst was pre-reduced at a  
269 temperature range of 400-600°C, which had a major impact on the catalytic performance with  
270 an increase of the temperature. At 500 °C reaction temperature and 600°C reduction  
271 temperature, NH<sub>3</sub> conversion was above 90 % and after 6 consecutive runs CoRe<sub>1.6</sub> presented  
272 excellent stability with no significant changes in the structure except the partial oxidation and  
273 re-reduction of the Co particles that acts in favour on the restart of the NH<sub>3</sub> decomposition.

274 Potassium promoted iron catalysts supported on carbon (K<sup>+</sup>-Fe/C) were studied by Jedynek et  
275 al. [62] to show the influence of the iron particle sizes on the rate of ammonia decomposition.  
276 Results showed that smaller particles gave higher TOFs in contrast with larger particles. K<sup>+</sup>-  
277 Fe<sub>5.7</sub>/C (12.5 nm) gave a TOF value of 0.5 s<sup>-1</sup> in contrast with the K<sup>+</sup>-Fe<sub>24</sub>/C (24 nm) that  
278 displayed a TOF value of 0.25 s<sup>-1</sup> concluding, that the smaller the surface of iron crystallites is,  
279 the more advantageous are the catalytic properties.

280 Ganley et al. [63] examined 13 metallic catalysts (Ru, Ni, Rh, Co, Ir, Fe, Pt, Cr, Pd, Cu, Te,  
281 Se, Pb) supported on pellets of activated alumina in order to suggest potential alternatives of  
282 Ru catalysts due to their high cost. Ru was the most active catalyst and besides Ni that had 40%  
283 lower activity than Ru, all the others were not efficient for the ammonia decomposition  
284 reaction. Also, depending on the catalyst that is used, the rate limiting step differs regarding  
285 nitrogen desorption or N-H bond scission. This suggests that is unlikely to predict catalytic

286 behaviour using only one parameter by assuming that a range of metallic catalysts have the  
287 same rate determining step for a given reaction.

288 Carbon nanotubes (CNTs) with residual Co or Fe nanoparticles were used as catalysts by Zhang  
289 et al. [64] for ammonia decomposition. With an increase in the temperature, ammonia  
290 conversion also increased and even at higher temperatures such as 700 °C the chemical  
291 composition and microstructure of CNTs remained the same as it was before the reaction took  
292 place. Fe containing CNTs had an activation period of 1200 min with a conversion up to 76 %  
293 but Co containing CNTs showed the highest activity overall with a conversion almost up to  
294 100 %. The higher activity of Co-containing CNTs might be due to their smaller particle size  
295 (4-20 nm) when compared with Fe-containing particles that were 10-50 nm, and the capacity  
296 of CNTs as electron reservoirs.

297 El-Shafie et al. [65] developed zeolite (SA-600A)-based catalysts with Ru and Li as supporting  
298 materials at different mixing ratios for H<sub>2</sub> generation from ammonia decomposition. For all the  
299 developed catalysts it was observed that increasing the temperature the conversion rate  
300 increased as well. It was observed that the catalyst was enhanced when the Li mixing ratio was  
301 increased, and the highest NH<sub>3</sub> conversion rate (99.9%) was obtained from the catalyst with a  
302 Li mixing ratio of 4 %. The increase of Ru ratio enhanced the conversion rate even more at  
303 lower temperatures. The catalyst with mixing ratio of 40 g (SA-600A)/5 g RuCl<sub>3</sub>.nH<sub>2</sub>O/3 g  
304 LiOH·H<sub>2</sub>O obtained the highest catalytic activity and NH<sub>3</sub> conversion of 99.87 % at 490 °C.

305 Core-shell iron-based catalysts ( $\alpha$ -FeO<sub>2</sub>O<sub>3-x</sub>@pSiO<sub>2</sub>) were synthesized for ammonia  
306 decomposition by Feyen et al. [66]. The catalysts were found to be highly stable up to  
307 temperatures of 800 °C with higher reaction rates and full conversion for all the tested catalysts.  
308 Moreover, particle sizes between 35 and 75 nm showed a limited influence on the catalytic  
309 activity. Lastly, there were no diffusion limitations up to flow rates of 120000 cm<sup>3</sup> g<sub>cat</sub><sup>-1</sup> h<sup>-1</sup> that  
310 could have been observed from the porous silica shells.

311 Cobalt catalysts supported on different carbon materials were developed for H<sub>2</sub> production  
312 from ammonia decomposition by Zhang et al. [67]. The carbon materials that were utilized for  
313 the research were multi-walled carbon nanotubes (MWCNTs), single wall carbon nanotube  
314 (SWCNTs), three types of activated carbons (AC) and reduced graphene oxides (RGO). The  
315 highest NH<sub>3</sub> conversion was conducted by the Co/MWCNTs catalyst. The conversion of  
316 Co/RGO and Co/SWCNTs catalysts was very low and therefore they weren't used for further  
317 studies. Moreover, the influence of post-treatment temperature on the catalytic performance of

318 10Co/MWCNTs (10% wt Co) was evaluated in this study at a temperature range of 230-700  
319 °C. Highest TOF value was obtained at 600 °C and it reached up to 8.15 s<sup>-1</sup>. Even after 20 h of  
320 catalytic test there was no significant change in the Co particle size. The fresh catalyst had a  
321 mean size of 4.8 nm while the used catalyst had 5.6 nm. Due to its higher catalytic stability and  
322 the excellent catalytic activity for the decomposition of ammonia, Co/MWCNTs catalyst could  
323 be promising for future applications.

324 Catalysts with 2 % Ru content supported on lanthania-ceria materials with different molar  
325 ratios were synthesized by Le et al. [68] to evaluate the H<sub>2</sub> production by ammonia  
326 decomposition. The catalytic activity was tested at temperature range of 300-500 °C and the  
327 Ru/La<sub>0.33</sub>Ce<sub>0.67</sub> exhibited the best catalytic performance with an ammonia conversion of 91.9  
328 % and H<sub>2</sub> formation rate of 6.2 mmol g<sub>cat</sub><sup>-1</sup> min<sup>-1</sup>. The acid-base properties of the La<sub>x</sub>Ce<sub>1-x</sub>O<sub>y</sub>  
329 supports combined with the high dispersion of Ru particles resulted in the enhanced catalytic  
330 activity. After 100 h the catalyst maintained its high catalytic activity due to its excellent  
331 stability, since fresh and used catalyst had a mean particle size of 3.3 nm and 3.6 nm  
332 respectively, showing no significant difference in the size and structural morphology of the  
333 particle.

334 Monometallic Ni, Co and bimetallic Ni-Co alloy catalysts supported on SiO<sub>2</sub> were prepared by  
335 a co-impregnation method by Wu et al [69]. Bimetallic catalysts had better catalytic  
336 performance obtaining higher ammonia conversion due to the alloy synergistic effect between  
337 Ni and Co. Among the tested catalysts, the Ni<sub>5</sub>Co<sub>5</sub>/SiO<sub>2</sub> exhibited the highest catalytic activity  
338 achieving 76.8 % NH<sub>3</sub> conversion and H<sub>2</sub> formation rate of 25.71 mmol g<sub>cat</sub><sup>-1</sup> min<sup>-1</sup> under  
339 GHSV of 30,000 mL h<sup>-1</sup> g<sub>cat</sub><sup>-1</sup> at 550 °C. The effect of GHSV was also examined showing that  
340 the increase of GHSV resulted the conversion decrease. With lower GHSV of 6000 mL h<sup>-1</sup> g<sub>cat</sub><sup>-1</sup>  
341 the catalyst achieved 94.7 % NH<sub>3</sub> conversion. Further enhancement on the conversion (78.1  
342 %) was observed when K was added during the Ni<sub>5</sub>Co<sub>5</sub>/SiO<sub>2</sub> synthesis (K/(Ni + Co) molar ratio  
343 of 1:10) indicating that alkali act in favour of the catalytic decomposition of ammonia. The  
344 Ni<sub>5</sub>Co<sub>5</sub>/SiO<sub>2</sub>-K was evaluated for its stability for 30 h where it showed negligible decrease in  
345 conversion and thus excellent stability.

346 Studies have reported that the stronger basicity of the support the more efficient is the catalyst  
347 and thus promoting the catalytic decomposition of ammonia. Therefore, Podila et al. [70]  
348 utilized different Mg oxide systems (MgAl, MgCe and MgLa) as supports for cobalt catalysts  
349 (5 wt% Co) with Mg to X (X = Al, Ce, La) ratio of 2. Among these three, 5CMLa-2 presented

350 the highest activity. The 5CMAI-2 and the 5CMCe-2 catalysts had lower activities. La-  
 351 containing catalysts were further studied with different Mg/La molar ratios (Mg/La = 1, 2,3,5,9  
 352 and 14). All the catalysts were active even at lower temperatures with 5CMLa-5 being the most  
 353 active. The higher activity of the 5CMLa-5 catalyst might be due to the increased surface area,  
 354 higher metal dispersion and the presence of basic sites that favour the ammonia decomposition.  
 355 It was concluded that Mg-La is a promising support for the reaction of ammonia  
 356 decomposition.

357 Pinzón et al. [71] developed Co catalysts supported on  $\beta$ -SiC for the H<sub>2</sub> production by ammonia  
 358 decomposition at reaction temperatures below 500 °C. The catalysts were modified with  
 359 different metals (K, Cs, Ca, Mg, La and Ce) to study the effect of promoters. The catalysts with  
 360 the addition of 1 % of Cs, Mg, Ca or Ce showed poorer performance while the catalysts loaded  
 361 with K or La enhanced the catalytic activity due their electron-donor properties that modified  
 362 the electronic structure of cobalt active sites. A conversion of 97.3 % and H<sub>2</sub> production rate  
 363 of 69.3 mmol H<sub>2</sub> g<sub>Co</sub><sup>-1</sup> min<sup>-1</sup> was obtained by the 1K-Co/SiC catalyst (4.1 wt % Co) at 450 °C.  
 364 Different K loadings were also studied, and results showed that the increase of metal loading  
 365 above 1% decreased the conversion of ammonia because the excess amount of metal blocked  
 366 the active sites of the cobalt catalysts. Lastly, the stability of the catalyst was tested for over 24  
 367 h at 400 °C and 83 % conversion of ammonia was reached providing excellent stability.

368 Table 1. Heterogeneous catalysts used for the ammonia decomposition.

Catalyst	Temperature (°C)	Conversion (%)	TOF (1/s)	Reference
Ni/MgAl <sub>2</sub> O <sub>4</sub> – LDH	600	88.7	2.18	[56]
Co/NC-600	500	80		[57]
Ru/SmCeO <sub>x</sub>	400	74.9	25.81	[58]
35Co/BHA	500	87.2		[59]
2.5Ru/10C-rGO	400	96	75.4	[60]
CoRe <sub>1.6</sub>	500	~90		[61]
K <sup>+</sup> -Fe/C	470	20	~0.5	[62]
Ru/Al <sub>2</sub> O <sub>3</sub>	580		6.85	[63]
Ni/Al <sub>2</sub> O <sub>3</sub>	580		4.21	[63]
Co-containing CNTs	700	~100		[64]
Fe-containing CNTs	700	76		[64]
(SA-600A)/RuCl <sub>3</sub> .nH <sub>2</sub> O/LiOH·H <sub>2</sub> O (40:5:3)	490	99.87		[65]
$\alpha$ -FeO <sub>2</sub> O <sub>3</sub> -50@pSiO <sub>2</sub>	800	100		[66]
10% Co/MWCNTs	600		8.15	[67]
Ru/La <sub>0.33</sub> Ce <sub>0.67</sub>	450	91.9	11.4	[68]
Ni <sub>5</sub> Co <sub>5</sub> /SiO <sub>2</sub>	550	76.8		[69]
5CMLa-5	550	82.7		[70]

1%K-Co/SiC	350	33.1	9.3	[71]
1%K-Co/SiC	450	97.3		[71]

369 As observed from Table 1, the temperature ranges from 400 to 800 °C because ammonia  
370 requires higher temperatures for its decomposition. At higher temperatures the conversion is  
371 higher and in some cases the catalysts achieve almost complete conversion. Even though Ru is  
372 a precious and expensive metal, many studies have focused on Ru catalysts due to their  
373 excellent catalytic properties [58], [60], [63], [65], [68] . However, other novel catalysts are  
374 investigated with promising results for future experiments [56], [59], [61], [64], [71].  
375 Supporting materials are also studied because of their properties for enhanced catalytic  
376 operation as they can offer higher surface area, chemical stability and mechanical strength [72].  
377 Generally, the most common ones are alumina and silica [63], [69], but other materials are used  
378 as well [57]–[60], [67], [71].

#### 379 **4.1.1 Structural and physicochemical properties of heterogeneous catalysts**

380 It's necessary to consider any chemical and physical transformation that will occur during the  
381 development process of efficient catalysts. The structure and properties of the catalysts play a  
382 significant role for the decomposition of any reaction. It is well known that the catalytic  
383 decomposition of ammonia is structure sensitive and strongly depends on the size, shape and  
384 properties of the catalyst. Mazzone et al. [73] synthesized unpromoted and sodium promoted  
385 Ru particles supported on carbon xerogels. The purpose of this study was to investigate the  
386 behaviour of the catalysts with support and with or without the promoter. During the second  
387 reaction run the un-promoted catalysts exhibited higher reaction rates compared with the first  
388 reaction run. The authors explained that the higher reaction rates are due to the formation of  
389 B5 sites after the catalyst was exposed at 600°C. The B5 sites work in favour of the  
390 decomposition reaction, speeding up the N desorption. Sodium as a promoter had a positive  
391 effect on the performance of the catalyst preventing the sintering of the Ru particles since the  
392 catalyst before and after five runs had the same average particle size for all tested catalysts. In  
393 contrast, the un-promoted catalysts presented a slight increase in the particle size, e.g., from  
394 1.9 nm to 2.5 nm due to the sintering of Ru particles from high temperatures. The support was  
395 either activated with carbon dioxide or doped with nitrogen and both treatments had a positive  
396 impact on the catalytic performance.

397 The effect of particle size was examined by El-Shafie et al. [74] using two different diameters  
398 of alumina particles size (1 and 2 mm) for the decomposition of ammonia assisted by dielectric

399 discharge plasma (DBD). The conversion rates and H<sub>2</sub> concentration were measured at different  
400 ammonia flow rates and plasma voltage. Conversion rates of 83.19 and 80.35 % were obtained  
401 by Al<sub>2</sub>O<sub>3</sub> particle sizes of 1 and 2 mm respectively. Moreover, particle size of 1 mm resulted  
402 in higher H<sub>2</sub> concentration. The higher conversion and H<sub>2</sub> concentration are attributed to the  
403 higher surface area in the smaller particle and thus, longer residence time for the decomposition  
404 reaction. Therefore, it was concluded that the particle size is a significant factor for this  
405 catalytic decomposition.

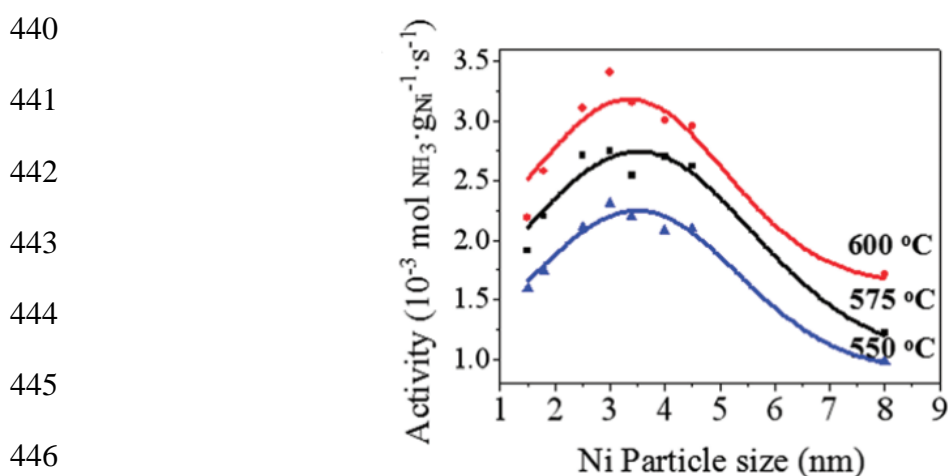
406 Cobalt catalysts in the form of cobalt oxide (II III) promoted with calcium, aluminium and  
407 potassium oxides were developed with precipitation method by Czekajło et al. [75]. With the  
408 increase in the precipitation process temperature, it was observed that the size of Co<sub>3</sub>O<sub>4</sub>  
409 crystallites was reduced leading to a decrease of the efficiency process. The ZBAP1-C catalyst  
410 that was promoted with calcium, potassium, and aluminium oxides obtained the highest  
411 catalytic activity with a decomposition degree of 100% at 525°C. The addition of alumina had  
412 a positive effect on a shift of the maximum conversion of ammonia towards lower reaction  
413 temperatures. The ZBAP1-B catalyst had the lowest surface area value impregnated only with  
414 oxides of calcium and potassium while the ZBAP1-C catalyst showed higher resistance in  
415 sintering indicating that the addition of aluminium has a positive impact on the stability of the  
416 surface structure as well.

417 Fly ash (FA), a waste material, was used as support for Ru catalysts for H<sub>2</sub> production by  
418 ammonia decomposition by Li et al. [76]. The FA samples were acid treated and heat treated,  
419 and results showed that treatment enhanced the surface area and pore volume. Ru impregnation  
420 further increased the surface area and pore volume on the heat treated and untreated FA samples  
421 but decreased on the acid treated samples. From the catalysts used, Ru/FA-800 had the highest  
422 conversion of ammonia due to high Ru dispersion, less acid sites and stronger NH<sub>3</sub> adsorption.

423 Lenzion-Bielun et al. [77] examined the effect of different promoters (CaO, Al<sub>2</sub>O<sub>3</sub> and, K<sub>2</sub>O)  
424 and also the addition of manganese and chromium on the structure of cobalt catalysts for  
425 ammonia decomposition. Sintering of pure cobalt was noticed at a temperature of 600°C, but  
426 with the addition of the oxides as promoters the surface area of the catalysts was stabilized.  
427 The catalytic tests showed that the unpromoted Co catalyst has the lowest activity due to a very  
428 low surface area. The Co(0) catalyst that was promoted with the oxides (2.6 wt % Al<sub>2</sub>O<sub>3</sub>, 1.5  
429 wt % CaO, 0.5 wt % K<sub>2</sub>O and 95.4 wt % Co) presented the highest activity at temperatures of  
430 500 and 550°C with NH<sub>3</sub> conversion up to 40.1 and 50% respectively. Even though an addition

431 of chromium and manganese lead to an enhancement on the surface area of the catalyst, the  
432 activity was decreased.

433 To investigate the influence of particle size, Li et al. [78] developed Ni particles supported on  
434 MCF-17 with particle range size from 1.5 to 8.0 nm. The ammonia decomposition reaction was  
435 affected by the particle size of the catalysts especially with small Ni particles. Moreover, the  
436 particle size effect was studied at various temperatures and a volcano relationship between the  
437 particle size and the catalytic activity was obtained (Fig.6) proving that the catalysts are  
438 structural sensitive. The Ni/MCF-17 catalyst with an average of 3.0 nm particle size exhibited  
439 excellent catalytic performance at all temperatures.



447 Fig.3. Effect of the particle size at different reaction temperatures [78].

448 Besides the correlation between the particle size of catalysts and the catalytic activity, the  
449 structure/morphology of the support is important to be explored. Huang et al. [79] studied  
450 cobalt catalysts supported on three kinds of CeO<sub>2</sub> supports, 3D ordered mesoporous (3DOM),  
451 nanotubes (NT) and nanocubes (NC). The Co/CeO<sub>2</sub>-3DOM catalyst exhibited the best catalytic  
452 performance with 4.2 mmol H<sub>2</sub> min<sup>-1</sup> g<sub>cat</sub> H<sub>2</sub> production rate at 500°C. According to different  
453 characterization techniques that were used in the experiment it was concluded that the particle  
454 size was not the main factor to influence the reaction but the different morphologies of the  
455 support. The morphology of the Co/CeO<sub>2</sub>-3DOM catalyst was favourable for construction of  
456 more active sites and thus the better catalytic performance.

## 457 4.2 Photocatalysis and Electrocatalysis of Ammonia

458 Photocatalytic decomposition is considered a promising system for the H<sub>2</sub> production because  
459 it can be operated at ambient temperature conditions, and the reaction can be easily controlled



460 by switching on and off the light irradiation [80]–[83]. TiO<sub>2</sub> photocatalysts were developed by  
461 Abdul Razak et al. [84] that were impregnated with Pd and Cu respectively for enhancement  
462 of the photocatalytic activity. After 3 h of light irradiation Pd/TiO<sub>2</sub> exhibited the highest  
463 activity producing 65 μmol of H<sub>2</sub> while Cu/TiO<sub>2</sub> and TiO<sub>2</sub> showed almost no production of H<sub>2</sub>.  
464 For the investigation of the stability of the photocatalysts in alkaline conditions, different NH<sub>3</sub>  
465 concentrations were investigated. With a concentration up to 19.1 g/L yield was enhanced up  
466 to 30.4 μmol but further increase of NH<sub>3</sub> resulted in a decline of the H<sub>2</sub> production rate.  
467 Dimethyl sulfoxide (DMSO) was also added as hydroxyl scavenger in ammonia further  
468 enhancing the H<sub>2</sub> yield to 121 μmol and was continuously increasing in the first cycle reaction.  
469 However, the rate of H<sub>2</sub> production was reduced with the subsequent reaction cycles and during  
470 the photocatalytic decomposition with DMSO methane gas was detected.

471 Apart from catalysis and photocatalysis, electrochemical decomposition of ammonia has a high  
472 potential for supply of CO<sub>x</sub>-free energy. Fig.3 demonstrates a typical ammonia electrolytic cell  
473 for hydrogen generation. The most active catalyst for this reaction is Pt and thus lots of research  
474 was carried out with Pt catalysts. However, it is very expensive so recent studies are focused  
475 on Pt-free catalysts [85]–[87]. Binary alloy electrocatalysts based on Ni such as NiCo, NiMo,  
476 NiFe, and NiCe deposited on nickel foam were synthesized by Jiang et al. [88] for the  
477 electrochemical generation of H<sub>2</sub> by ammonia. From all the electrodes investigated, NiCo in  
478 the form of nanoneedle resulted in an impressive electrochemical performance. For further  
479 improvement the NiCo catalyst was introduced to nitrogen doping and ammonia annealing  
480 treatment to obtain NiCo<sub>2</sub>N electrodes. The activity was dramatically increased demonstrating  
481 a superior HER electrocatalytic performance. The NiCo<sub>2</sub>N electrocatalysts also showed an  
482 excellent stability as there was no significant change after 10 h of catalytic process. Moreover,  
483 it was concluded that the electrolysis potential in ammonia (0.71 V) was much lower than the  
484 water splitting suggesting that ammonia electrolysis can replace water electrolysis for H<sub>2</sub>  
485 production. Table 2 summarises the results from photocatalysis and electrocatalysis of  
486 ammonia.

487

488

489

490

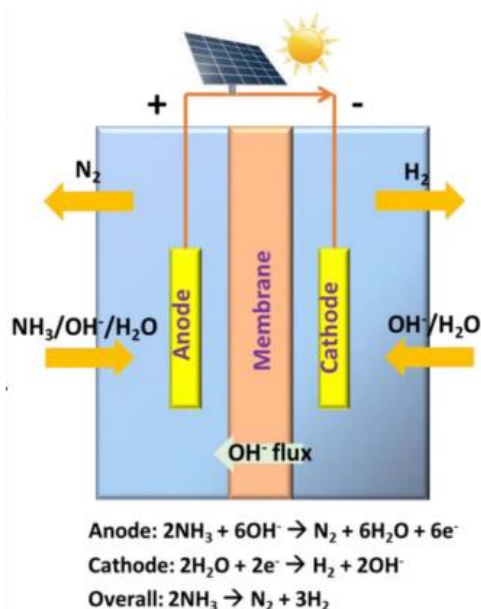
491

492

493

494

495



496 Fig.4. A typical cell of ammonia electrolysis for hydrogen production [87].

497 Table 2. Photocatalysts and Electrocatalysts used for ammonia decomposition.

Photocatalysis				
Catalyst	H <sub>2</sub> Yield (μmol)			Reference
Pt/TiO <sub>2</sub>	160			[80]
Pt/Fe-TiO <sub>2</sub>				[81]
Ce/TiO <sub>2</sub>	80			[82]
Pd/TiO <sub>2</sub>	65			[84]
Pd/TiO <sub>2</sub> -DMSO	121			[84]
Electrocatalysis				
Catalyst	System	Onset Potential	Current Density (mA cm <sup>-2</sup> )	Reference
NiCu/C	55mM NH <sub>4</sub> Cl + 0.5 NaOH	0.47 V vs Ag/AgCl	52	[85]
Ni <sub>98</sub> Pd <sub>2</sub>	1M NaNO <sub>3</sub> + 200mM NH <sub>4</sub> NO <sub>3</sub> + NaOH	1.25 V vs Hg/HgO	~2	[86]
NiCo <sub>2</sub> N	1M KOH + 1M NH <sub>3</sub> .H <sub>2</sub> O	100x10 <sup>-3</sup> V vs RHE	100	[88]

498

## 499 **5 Hydrous Hydrazine Decomposition as a sustainable hydrogen** 500 **production method**

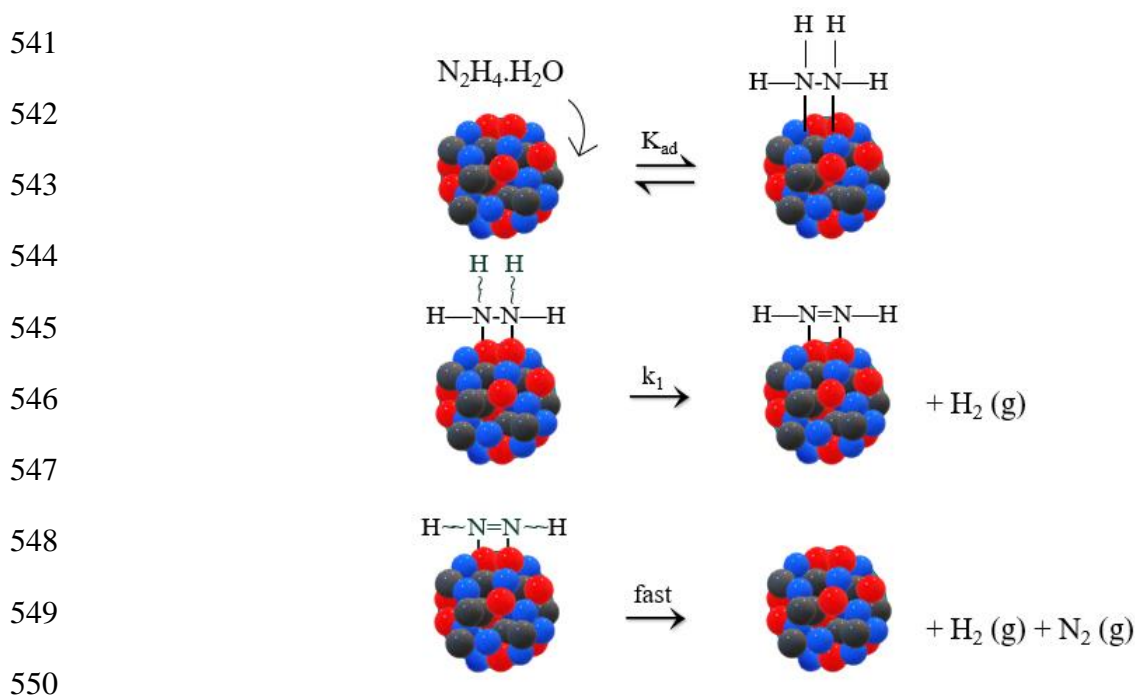
### 501 **5.1 Heterogeneous Catalysis of Hydrous Hydrazine**

502 In recent years, the development of efficient catalysts for the decomposition of hydrous  
503 hydrazine for H<sub>2</sub> generation has been the focus of many studies. Ni particles were found to be  
504 a preferable choice and its alloying with noble metals such as Ir, Pt, Pd and Rh result in a  
505 noteworthy improvement on the H<sub>2</sub> selectivity and the catalytic performance due to the alloy  
506 synergistic effect [89]–[91]. Unfortunately, their applications are limited due to the high cost  
507 of noble metals. Therefore, it is essential to develop non noble metal containing catalysts. Until  
508 now, many studies have reported the decomposition of hydrous hydrazine with noble-metal-  
509 free catalysts. Different types of catalysts that were used for the decomposition of hydrous  
510 hydrazine are displayed in Table 3.

511 Noble-metal-free NiFe particles supported on CeZrO<sub>2</sub> were synthesized by Zoo et al. [92]. The  
512 NiFe/CeZrO<sub>2</sub> alloy catalyst with Ni/Fe molar ratio of 8:2 (9.11 wt % Ni and 2.41 wt % Fe) had  
513 a TOF value of 119.2 h<sup>-1</sup> and 100% H<sub>2</sub> selectivity in the presence of NaOH and temperature  
514 of 343 K. The catalyst exhibited high stability showing negligible decrease on the H<sub>2</sub> selectivity  
515 after five runs. The particle size of the NiFe/CeZrO<sub>2</sub> catalyst was 5.2 ± 0.8 nm while after five  
516 runs was 5.3 ± 1.2 nm. Other supports as LaZrO<sub>2</sub> and NdZrO<sub>2</sub> also presented excellent catalytic  
517 properties. NiCo, NiCu and CoFe supported on CeZrO<sub>2</sub> were also examined and exhibited  
518 lower selectivity towards H<sub>2</sub> concluding that NiFe is a highly efficient candidate for the  
519 replacement of noble metal catalysts for the hydrous hydrazine decomposition.

520 Liu et al. [93] synthesized NiMo particles supported on TiO<sub>2</sub> for the catalytic decomposition  
521 of hydrous hydrazine. The Ni<sub>0.16</sub>Mo<sub>0.04</sub>/TiO<sub>2</sub> catalyst with 22.6 wt % Ni and 9.23 wt % Mo  
522 exhibited a TOF value of 484 h<sup>-1</sup> and 100% H<sub>2</sub> selectivity. Further increase of the support  
523 content decreased the catalytic performance, After, 10 cycles the selectivity remained 100%  
524 but the TOF decreased to 138 h<sup>-1</sup>. NiCu/TiO<sub>2</sub>, NiFe/ TiO<sub>2</sub>, and NiCo/TiO<sub>2</sub> catalysts were also  
525 prepared for investigation of doping other metals and results showed that the catalytic  
526 performances of these catalysts were inferior to NiMo/TiO<sub>2</sub> concluding that Mo doping  
527 improves the dispersion and modifies the geometric and electronic structure of the catalyst  
528 facilitating the N<sub>2</sub>H<sub>4</sub> decomposition.

529 Mono-, bi- and tri-metallic noble and noble-metal free catalysts were prepared by Al-Thubaiti  
 530 et al. [94] to investigate their catalytic activity in the dehydrogenation of hydrous hydrazine.  
 531 Monometallic Ag, Ni, Pd, Fe and Cu particles were inactive while the activity of bimetallic  
 532 catalysts was higher. The most active catalyst was the trimetallic Ni/Fe/Pd catalyst that  
 533 contained 28.7 wt % Ni, 23.5 wt % Fe and 47.7 wt % Pd and average size of 20 nm. It exhibited  
 534 excellent selectivity towards H<sub>2</sub> and therefore was used for further experiments. After five  
 535 continuous runs the catalytic activity of the catalyst remained the same. It was concluded by  
 536 the authors that adding a third metal in a bimetallic catalyst with a specific combination has a  
 537 positive impact on the selectivity of H<sub>2</sub>. Fig.5 shows the proposed mechanism for the  
 538 decomposition of ammonia on the surface of the Ni/Fe/Pd catalyst. Moreover, new catalysts  
 539 can be developed with different metal plating order for the decomposition of hydrazine for H<sub>2</sub>  
 540 production.



551 Fig.5. Decomposition mechanism of hydrous hydrazine on the surface of the trimetallic  
 552 Ni/Fe/Pd catalyst [94].

553 Different elements (Rh, Co, Ru, Ir, Cy, Ni, Fe, Pt, Pd NPs) were studied as catalysts for the  
 554 decomposition of hydrous hydrazine for H<sub>2</sub> production by Sanjay et al. [95]. It was found that  
 555 the catalytic activity and the selectivity were depended on the catalyst used. Rh was the most  
 556 active catalyst whereas Cu, Ni, Fe, Pt and Pd were inactive for the reaction in aqueous solution  
 557 even though they were active in the reaction that took place in the gas-phase. In the case of Co,

558 Ru and Ir the selectivity towards H<sub>2</sub> was very low. The reason this is happening is because Co,  
559 Ru and Ir nanoparticles prefer the activation of the N-N bond which is formatting ammonia. In  
560 comparison Rh particles prefer the activation of N-H bond and that's why they are highly  
561 active. Moreover, it was observed that the catalytic activity was enhanced when the Rh particles  
562 were reduced with NaBH<sub>4</sub> in the presence of hexadecyltrimethyl ammonium bromide  
563 concluding that the modification of nanoparticles during their preparation could affect their  
564 efficiency.

565 Motta et al. [96] investigated the catalytic performance of Ir/CeO<sub>2</sub> as catalyst for the  
566 decomposition of hydrous hydrazine to generate H<sub>2</sub>. Parameters such as stirring speed, mass of  
567 catalyst, NaOH concentration and reaction temperature were studied to find the optimal  
568 conditions for the reaction with respect on the activity and selectivity of the catalytic  
569 decomposition. Stirring rate affected both the reaction rate and the selectivity and it was found  
570 that with lower stirring rate the H<sub>2</sub> yield was also lower. The optimum stirring rate was 1050  
571 rpm and was used for the following tests. The mass of the catalyst did not affect the yield of  
572 the reaction but there was an increase in the activity for molar ratios between 125:1 and 250:1  
573 and the latter were selected for the further catalytic tests. With an increase of the NaOH  
574 concentration there was an increase in H<sub>2</sub> yield and 0.5 M NaOH was chosen as the optimal  
575 value. Lastly, with an increase in the temperature the selectivity decreased in contrast with the  
576 activity of the catalyst that was increased so the value of 50°C was chosen because of the  
577 intermediate values of activity and selectivity that exhibited. The fresh catalyst had a particle  
578 size of  $0.9 \pm 0.2$  nm and after five uses  $1.2 \pm 0.4$  nm where the difference was in the range of  
579 the error analysis.

580 Kang et al. [97] developed Ni/CeO<sub>2</sub> catalysts for the decomposition of hydrous hydrazine. A  
581 solution combustion synthesis (SCS) varying different parameters was used to synthesize the  
582 catalysts and catalytic tests were run under 50°C. It was obtained that catalysts with smaller Ni  
583 size particle and larger pore size act in favour of the decomposition resulting in a good catalytic  
584 performance. 6 wt% Ni/CeO<sub>2</sub> catalysts with 14.7 nm particle size and 18.8 nm pore size,  
585 exhibited a H<sub>2</sub> selectivity of 100 %, N<sub>2</sub>H<sub>4</sub>.H<sub>2</sub>O conversion of 50 % at 17.7 min corresponding  
586 to a TOF value of 34.0 h<sup>-1</sup>. Moreover, the formation of Ni-O-Ce solid promoted the reaction  
587 for H<sub>2</sub> generation, but higher concentrations decreased the catalytic activity. A 30-fold increase  
588 of the reaction rate was obtained when increasing the temperature from 30 to 90°C but the  
589 selectivity dropped at 93 %. Lastly, for comparison purposes, Ni-based catalysts developed

590 with different methods were tested and even though a high number of parameters need to be  
591 considered, it was concluded that the catalysts created by the SCS method had better catalytic  
592 performance.

593 An alloy of Ni-Pd nanoparticles ( $\text{Ni}_{1-x}\text{Pd}_x$ ) were synthesized by Singh et al. [98] and were  
594 examined under mild reaction conditions. The  $\text{Ni}_{0.60}\text{Pd}_{0.40}$  catalyst exhibited the highest  
595 selectivity (82 %) among the others tested. To test the effect of alloy, a physical mixture of Ni  
596 and Pd was tested and performed poor catalytic activity compared with the alloy catalyst  
597 indicating that the modified catalyst surface favours this reaction. The combination of Pd with  
598 other metals (Fe, Co and Cu) resulted poor catalytic performance (or inactive) as well as  
599 implying that the presence of Ni has a positive effect on the decomposition of hydrous  
600 hydrazine.

601 He et al. [99] developed Ni-based catalysts by using Ni-Al hydrotalcite-like compound as  
602 precursors. A conversion of 100 % was exhibited with a  $\text{H}_2$  selectivity of 93 % at 30 °C and 70  
603 min reaction time. The high selectivity can be attributed to the small Ni particles and strong  
604 basic sites. When the temperature increased up to 80 °C, the reaction time decreased at 5 min  
605 and the selectivity was reduced to 82 %. A Ni/ $\text{Al}_2\text{O}_3$ -IMP catalyst was also tested for the  
606 decomposition of hydrous hydrazine and compared with Ni- $\text{Al}_2\text{O}_3$ -HT. A lower activity was  
607 noticed by the Ni/ $\text{Al}_2\text{O}_3$ -IMP catalyst with  $\text{H}_2$  selectivity at 66 % and 440 min of reaction time  
608 due to the poor Ni dispersion.

609 Amorphous catalytic CoPt particles induced on CeOx were developed by Song-II et al. [100].  
610 It was discovered that the CeOx plays a crucial role in the transformation of the crystalline  
611 phase to the amorphous one. The highest catalytic performance among the catalysts tested was  
612 achieved by the  $\text{Co}_{0.65}\text{Pt}_{0.30}(\text{CeOx})_{0.05}$  nanoalloy, at 25 °C with  $\text{H}_2$  selectivity of 72.1 % in 3.5  
613 min and TOF value of  $194.8 \text{ h}^{-1}$  which is even higher than that of the crystalline phase catalyst.  
614 Therefore, it was concluded by the authors that  $\text{Co}_{0.65}\text{Pt}_{0.30}(\text{CeOx})_{0.05}$  exhibited the most  
615 optimum performance encouraging its practical use for the decomposition of  $\text{N}_2\text{H}_4 \cdot \text{H}_2\text{O}$  to  
616 produce  $\text{H}_2$ .

617 Several studies used RhNi alloy catalysts supported on different materials for the  
618 decomposition of hydrous hydrazine. Zhang et al. [101] developed CeOx-doped RhNi particles  
619 supported on reduced graphene oxide (rGO). The  $\text{Rh}_{0.8}\text{Ni}_{0.2}@\text{CeOx}/\text{rGO}$  catalyst completely  
620 decomposed  $\text{N}_2\text{H}_4$  at room temperature in 33 min with a TOF value of  $36.4 \text{ h}^{-1}$ . Further increase  
621 in the temperature at 60°C, catalysed the reaction in 3.0 min giving a TOF value of  $400.0 \text{ h}^{-1}$ .

622 Other studies used MOFs for the support of catalytic materials and therefore RhNi@MIL-101  
623 [102] and NiRh/NPC-900 [103] were developed and tested at 50 °C and alkaline conditions 0.5  
624 NaOH. High TOF values of 344 h<sup>-1</sup> and 156 h<sup>-1</sup> were exhibited respectively with 100 % H<sub>2</sub>  
625 selectivity. Other supports that were used in these studies presented inferior catalytic  
626 performance.

627 Dai et al. [104] synthesized bimetallic Ni-Ir alloy nano-catalysts supported on CeO<sub>2</sub> for the  
628 decomposition of hydrous hydrazine for H<sub>2</sub> production. The catalyst showed great catalytic  
629 activity and high H<sub>2</sub> selectivity. Further increase on the Ir content (Ni<sub>91</sub>Ir<sub>9</sub>/CeO<sub>2</sub>) resulted in an  
630 optimal catalytic performance and was further investigated. The decomposition rate of hydrous  
631 hydrazine increased with increasing the reaction temperature. Also, the catalyst was submitted  
632 to cyclic usage, and it was found that it retains 100% H<sub>2</sub> selectivity even after 15 cycles but the  
633 catalytic activity was decreasing after cycle.

634 Nickel particles were prepared by encapsulation in the channel of TNTs (Ni@TNTs) and  
635 deposition on the surface of TNTs (Ni/TNTs) by Wang et al. [105]. Ni@TNTs exhibited high  
636 catalytic activity than the Ni/TNTs catalyst and nearly 100% H<sub>2</sub> selectivity at 333 K. The TOF  
637 value of this reaction was 96.0 h<sup>-1</sup>. The encapsulation of Ni particles led to a small particle size  
638 of 2.7 nm, large pore size of 10.2 nm and high dispersion (28.2 %) resulting in more active  
639 sites. Moreover, after six continuous catalytic runs the catalyst did not have any significant loss  
640 in its catalytic activity due to the prevention of nickel particles leaching during the catalysis,  
641 since the particle size had a small increase of 3.5 nm. In contrary, Ni particles on Ni/TNTs  
642 increased from 2.4 to 8.9 nm indicating that aggregation is occurring without the TNTs  
643 constraining the Ni particles.

644 Rh nanoparticles modified with Molybdenum Oxide (MoO<sub>x</sub>) were prepared by Yao et al. [106]  
645 with different metal compositions for the catalytic decomposition of hydrous hydrazine and  
646 hydrazine borane. Various reaction temperatures were studied and at temperature of 323 K and  
647 the presence of Rh<sub>0.5</sub>(MoO<sub>x</sub>)<sub>0.5</sub>, N<sub>2</sub>H<sub>4</sub> was completely decomposed to H<sub>2</sub> and N<sub>2</sub> with 100% H<sub>2</sub>  
648 selectivity and TOF value of 750 h<sup>-1</sup>. The catalyst had an average mean size of 3.8 ± 0.8 and  
649 its composition was 10.05 wt % Rh and 8.92 wt % Mo. It was concluded that the increased  
650 catalytic performance obtained by the Rh-based catalysts might encourage the utilisation of  
651 hydrous hydrazine as H<sub>2</sub> storage material.

652

653 Table 3. Heterogeneous catalysts utilized for the hydrous hydrazine decomposition.

Catalyst	Temperature (°C)	Conversion (%)	TOF (1/s)	Reference
Ni <sub>0.8</sub> Fe <sub>0.2</sub> /CeZrO <sub>2</sub>	70		0.033	[92]
Ni <sub>0.16</sub> Mo <sub>0.04</sub> /TiO <sub>2</sub>	70	~100	0.134	[93]
Ni/Fe/Pd	40		0.007	[94]
Ir/CeO <sub>2</sub>	50	~100	~0.028	[96]
6 wt% Ni/CeO <sub>2</sub>	50	50	0.009	[97]
Ni <sub>0.60</sub> Pd <sub>0.40</sub>	50			[98]
Ni-Al <sub>2</sub> O <sub>3</sub> -HT	30	100		[99]
Co <sub>0.65</sub> Pt <sub>0.30</sub> (CeOx) <sub>0.05</sub>	25		0.054	[100]
Rh <sub>0.8</sub> Ni <sub>0.2</sub> @CeOx/rGO	60	100	0.111	[101]
RhNi@MIL-101	50		0.095	[102]
NiRh/NPC-900	50	>50	0.043	[103]
Ni <sub>91</sub> Ir <sub>9</sub> /CeO <sub>2</sub>	50	100		[104]
Ni@TNTs	60	~100	0.026	[105]
Rh <sub>0.5</sub> (MoOx) <sub>0.5</sub>	50	100	0.208	[106]

654 Comparing with the temperature range of the ammonia decomposition, as seen from Table 3  
655 that hydrous hydrazine decomposition is more favored at lower temperatures (30-70 °C). The  
656 most studied temperature is 50 °C giving almost total conversion of hydrous hydrazine [96]–  
657 [98], [102]–[104], [106]. Nickel is a promising catalyst for this decomposition and by alloying  
658 it with other elements, many studies give positive results [92], [93], [97], [99], [105]. However,  
659 noble metals are often used for the alloys, limiting their application [94], [98], [101]–[104].  
660 Still research needs to be done though, considering the low TOF values.

### 661 5.1.1 Structural and physicochemical properties of heterogeneous catalysts

662 While the majority of studies are focused on the structure of the catalysts there was no in-depth  
663 study of the insights of the microstructure transformations during the synthesis of catalysts  
664 which are a key point for the catalytic activity for the hydrous hydrazine decomposition.  
665 Therefore Qiu et al. [107] synthesised Ni@Ni-Ir/meso-CeO<sub>2</sub> catalysts for the investigation of  
666 the catalytic properties that may be affected by the composition of the surface. Ni@Ir/ meso-  
667 CeO<sub>2</sub> resulted from the formation of the Ir surface layer on the Ni particles and with calcination  
668 treatment the targeted Ni@Ni-Ir/meso-CeO<sub>2</sub> alloy catalyst was synthesized. The post-treated  
669 alloy exhibited excellent activity with a reaction rate of 343 h<sup>-1</sup> and H<sub>2</sub> selectivity (100% H<sub>2</sub>)  
670 at 50°C, in contrast with the as-prepared catalyst that had lower selectivity and catalytic  
671 performance. It was concluded that the calcination treatment had a positive impact since the  
672 Ni@Ir alloy enhanced both the selectivity and catalytic activity.



673 Shi et al. [108] studied in detail the formation mechanism of the bimetallic Ni<sub>50</sub>Pt<sub>50</sub>/CeO<sub>2</sub> alloy  
674 for the investigation of the influence of preparation process to the structure of the catalyst and  
675 thus, the impact on catalytic activity. It was discovered that during the synthesis process the  
676 formation of [(CH<sub>3</sub>)<sub>4</sub>N]<sub>2</sub>PtCl<sub>6</sub> took place during the co-precipitation step. While increasing the  
677 aging time crystalline [(CH<sub>3</sub>)<sub>4</sub>N]<sub>2</sub>PtCl<sub>6</sub> disappeared due to the conversion to metallic Pt which  
678 was found to have a major impact on the composition and microstructure of the catalyst. As a  
679 result, the catalytic performance of the Ni<sub>50</sub>Pt<sub>50</sub>/CeO<sub>2</sub> catalyst was different depending on the  
680 aging time. After 5-12 h of aging time the reaction rate was 465-500 h<sup>-1</sup> at 30°C which was 2.5  
681 times higher than the reaction time of the catalysts with aging time of 0-1 h.

682 In another study by Shi et al. [109], noble metal free Ni-W-O alloy nano-catalysts  
683 (Ni<sub>4</sub>W/WO<sub>2</sub>/NiWO<sub>4</sub>) were synthesised with a hydrothermal process and different reduction  
684 temperatures to investigate any changes in the microstructure of the catalysts. Results showed  
685 that increasing the annealing treatment temperature the catalytic properties are increased as  
686 well. The reduction at 350°C showed both low selectivity and reaction rate while at 400°C  
687 selectivity was 99% and the reaction rate up to 33 h<sup>-1</sup> with a complete decomposition of  
688 hydrazine at 50°C and reaction time of 18 min. Further increase of the annealing treatment  
689 temperature reduced the efficiency of the catalyst. Moreover, different characterization  
690 analyses were used to better understand if the increased catalytic properties were correlated  
691 with the temperature treatment. A decrease on the specific surface area was obtained with the  
692 increased reduction temperature that led to the enhanced catalytic performance.

693 A Ni-Pt/La<sub>2</sub>O<sub>3</sub> catalyst was synthesised by Zhong et al. [110] combining alloying and  
694 immobilization strategies. The targeted Ni@Ni-Pt/La<sub>2</sub>O<sub>3</sub> contained a Ni core and Ni-Pt alloy  
695 shell and exhibited 100 % H<sub>2</sub> selectivity. A key factor to achieve great catalytic performance  
696 is the formation of the bimetallic alloy therefore the study was not only focused on the catalytic  
697 activity of the particles but also the physicochemical surface composition and structure. The  
698 excellent catalytic properties were correlated with the electronic and geometric structures  
699 changes during the Ni-Pt formation. Moreover, the catalysts were subjected into a second time  
700 replacement and calcination treatment under 350°C, and it was observed that both activity and  
701 selectivity towards H<sub>2</sub> were increased. It was found that not proper control of the calcination  
702 temperature can drastically reduce the performance of the catalyst. In general, there was a  
703 remarkable improvement after the treatment but still the reason behind the enhancement and  
704 the dependence of the treatment needs to be further studied.

705

### 5.1.2 NH<sub>3</sub> Formation

706 As it was mentioned hydrous hydrazine can be decomposed by two pathways resulting in the  
707 undesirable ammonia production. Thus is a necessity to develop effective catalyst with high  
708 selectivity towards H<sub>2</sub>. Ni catalysts alloyed with noble metals were a preferred choice by many  
709 researchers due to their remarkable enhancement of catalytic properties that resulted from the  
710 alloy synergy effect. For example, Singh et al. [91] developed bimetallic Ni-Pt alloy nano-  
711 catalysts to enhance the selectivity of Ni nanoparticles that was around 33 % at 323 K. By  
712 alloying Ni with Pt content as low as 1 mol % (Ni<sub>0.99</sub>Pt<sub>0.01</sub>), a complete conversion of N<sub>2</sub>H<sub>4</sub>·H<sub>2</sub>O  
713 was obtained in 120 min at 323 K. Further increase of the temperature at 333 K caused a  
714 reduction on the reaction time at 70 min with 100 % H<sub>2</sub> selectivity. Authors concluded that the  
715 Ni alloying with low Pt content and moderate temperatures are promising for the development  
716 of low-cost and high efficiency catalysts for H<sub>2</sub> production by hydrous hydrazine  
717 decomposition.

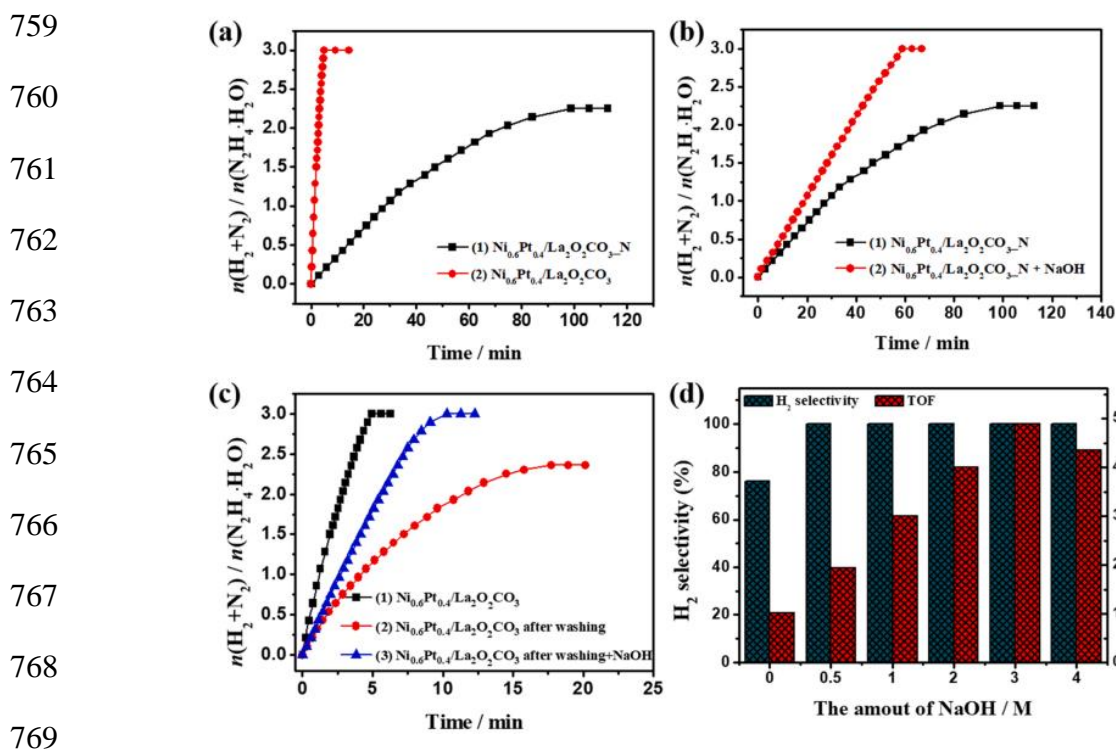
718 Ni-Ir alloy catalysts supported on Al<sub>2</sub>O<sub>3</sub> were investigated by He et al. [111] to compare its  
719 activity and selectivity with monometallic Ir/Al<sub>2</sub>O<sub>3</sub> and Ni/Al<sub>2</sub>O<sub>3</sub> catalysts. NiIr<sub>0.016</sub>/Al<sub>2</sub>O<sub>3</sub> (2.0  
720 wt % Ir, 36.8 wt % Ni and 6.1 wt % Al<sub>2</sub>O<sub>3</sub>) increased the selectivity up to 99 % and the reaction  
721 rate was 6.3 h<sup>-1</sup>. Increasing the Ir molar ratio to Ni up to 0.059, the reaction rate was enhanced  
722 at 12.4 h<sup>-1</sup> and selectivity remained higher than 98%. The stability of the NiIr<sub>0.059</sub>/Al<sub>2</sub>O<sub>3</sub> was  
723 tested at 10 consecutive cycles at 30°C. The reaction rate decreased to 9.2 h<sup>-1</sup> but the H<sub>2</sub>  
724 selectivity remained over 98%. Reduction of the catalyst at high temperatures resulted in a  
725 decreased selectivity and catalytic activity. Moreover, modified Au and Pt Ni/Al<sub>2</sub>O<sub>3</sub> catalysts  
726 were developed for comparison purposes. NiPt<sub>0.027</sub>/Al<sub>2</sub>O<sub>3</sub> exhibited high selectivity while  
727 NiAu<sub>0.020</sub>/Al<sub>2</sub>O<sub>3</sub> resulted in a lower selectivity and reaction rate as low as 2.0 h<sup>-1</sup>.

728 Furthermore, experiments showed that alkaline conditions lead to improved H<sub>2</sub> selectivity.  
729 Bimetallic nano-catalysts were developed by alloying Ni and Fe with different Ni/Fe molar  
730 ratios by Singh et al. [112] to investigate their catalytic performance for the decomposition of  
731 hydrous hydrazine. Even though the catalyst exhibited excellent catalytic activity, the  
732 selectivity towards H<sub>2</sub> was only 81%. With an addition of 0.5 M NaOH the selectivity was  
733 enhanced at 100%. The addition of NaOH also improved the selectivity of the Ni<sub>45</sub>Pt<sub>55</sub> and  
734 Ni<sub>50</sub>Ir<sub>50</sub> catalysts from 61 to 86% and from 7 to 95% respectively. It was suggested by the  
735 authors that the basicity of the NaOH makes the surface of the catalyst basic preventing the  
736 formation of NH<sub>3</sub> by the incomplete decomposition of hydrazine and thus promoting the first

737 pathway. Weaker bases such as ammonia and sodium acetate were also examined. Results  
738 showed that the addition of these bases had no effect on the catalytic activity and selectivity of  
739 the catalysts.

740 Ni particles were synthesised from the reduction of triangular  $\text{Ni}(\text{HCO}_3)_2$  nanosheets and were  
741 used as catalysts to produce  $\text{H}_2$  by hydrous hydrazine by Wang et al [113]. For the restraint of  
742 the  $\text{NH}_3$  formation as a side reaction, the effect of NaOH concentration was tested. It was found  
743 that with the absence of NaOH the selectivity towards  $\text{H}_2$  was 64.5%. With 0.5M of NaOH, the  
744 selectivity was up to 100% and remained unchanged with further increase of the NaOH  
745 concentration. Alkaline conditions speed up the rate determining step of the hydrous hydrazine  
746 decomposition and  $\text{OH}^-$  ions inhibit the formation of ammonia obtaining 100%  $\text{H}_2$  selectivity.

747 NiPt alloy nanoparticles supported on  $\text{La}_2\text{O}_2\text{CO}_3$  were developed via an alkali assisted  
748 reduction by Yao et al [114]. Among the catalysts tested the  $\text{Ni}_{0.6}\text{Pt}_{0.4}/\text{La}_2\text{O}_2\text{CO}_3$  (2.8 nm)  
749 obtained the best catalytic performance with a TOF number of  $490 \text{ h}^{-1}$  and 100 %  $\text{H}_2$  selectivity.  
750 After five rounds, the catalyst showed a good stability with only a slight aggregation of 3.4 nm.  
751 Further tests were conducted for the evaluation of NaOH effect at the synthesis of the catalysts  
752 and during the catalytic process. The catalyst prepared without the addition of NaOH exhibited  
753 much lower selectivity and catalytic performance even though NaOH was added during the  
754 decomposition reaction. Moreover, the catalyst was synthesised at different NaOH  
755 concentrations (0-4 M) and results showed that the efficiency of the catalyst increased until the  
756 NaOH concentration was 3 M. These results suggest that NaOH affects both the catalytic  
757 process and the preparation of the catalysts. The effect of the NaOH addition at the preparation  
758 step of the catalyst and during the process are presented below (Fig.6).



770 Fig.6. The effect of NaOH addition in the catalytic decomposition of  $\text{N}_2\text{H}_4\cdot\text{H}_2\text{O}$  [114].

771 Huang and Liu [115] examined both the synergistic effect from an Ni alloy and the addition of  
 772 NaOH to generate  $\text{H}_2$  from hydrous hydrazine. NiPt/C catalysts were synthesised with various  
 773 Pt/Ni molar ratios. The optimal catalytic activity was displayed by  $\text{Ni}_8\text{Pt}_1/\text{C}$  and used for further  
 774 studies with respect to different catalyst concentrations, initial  $\text{N}_2\text{H}_4$ , temperature and NaOH  
 775 concentration. With an increase on the catalyst concentration and initial  $\text{N}_2\text{H}_4$  the  
 776 dehydrogenation rate also increased. The catalytic activity slightly decreased after 5 catalytic  
 777 runs and characterization results showed that the average grain size of the reused catalyst  
 778 increased from 2.5 nm to 3.8 nm. At higher temperatures a higher TOF value was obtained.  
 779 Lastly, with an addition of 0.5 M NaOH, a TOF value of  $2640.5 \text{ h}^{-1}$  and 100 %  $\text{H}_2$  selectivity  
 780 were obtained at  $50^\circ\text{C}$ , while with no addition of the alkaline solution the TOF value was  $627.5$   
 781  $\text{h}^{-1}$ .

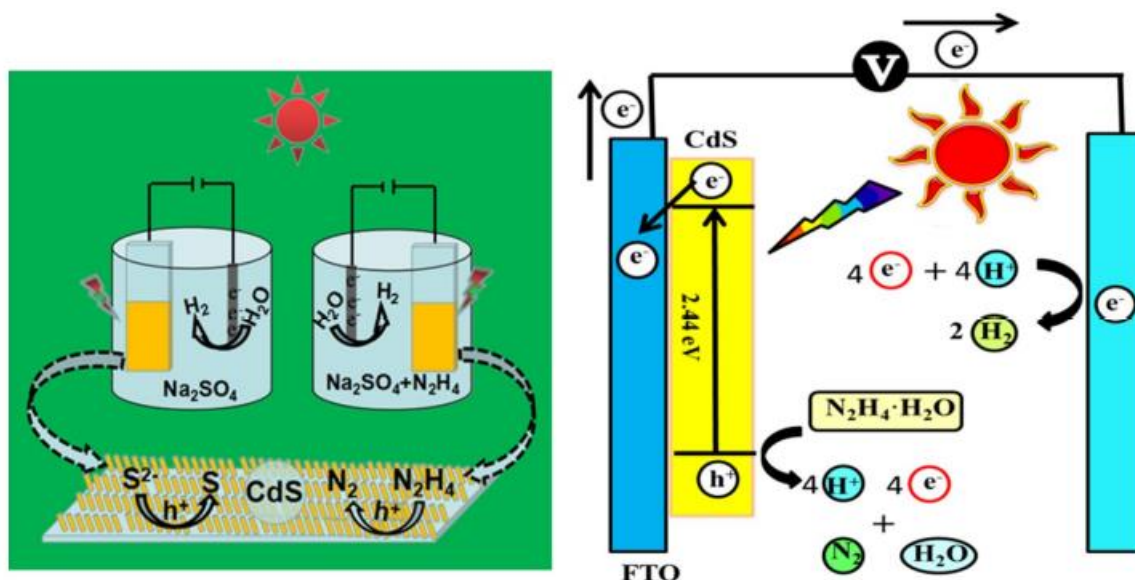
## 782 5.2 Photocatalysis and Electrocatalysis of Hydrous Hydrazine

783 The catalytic decomposition of hydrous hydrazine for the generation of  $\text{H}_2$  is well investigated,  
 784 but its photocatalytic decomposition still needs lots of research for the discovery of efficient  
 785 photocatalysts.  $\text{TiO}_2$  modified with deposition of noble metals is found to be very promising  
 786 as for the photocatalytic oxidation of hydrazine and its derivatives [116], [117].  $\text{TiO}_2$

787 nanoparticles modified with rhodium were developed by Kumar et al. [118] for the  
788 photocatalytic decomposition of hydrous hydrazine under visible light irradiation. Unmodified  
789 TiO<sub>2</sub> particles exhibited a H<sub>2</sub> production of 83 μmol g<sup>-1</sup> cat and formation rate of 6.9 μmol g<sup>-1</sup>  
790 cat h<sup>-1</sup> while TiO<sub>2</sub>-Rh had a H<sub>2</sub> production of 413 μmol g<sup>-1</sup> cat and rate formation 42.0 μmol g<sup>-1</sup>  
791 cat h<sup>-1</sup> after 12 h of visible light irradiation. The photocatalyst was still efficient after five  
792 subsequent runs and the H<sub>2</sub> yield was 384 μmol g<sup>-1</sup> cat but it was noticed a slight decrease in  
793 the photoactivity due to leaching of the Rh from the TiO<sub>2</sub> surface. After the five cycles, the  
794 value of Rh was 0.14 wt %, slightly lower than that of the fresh catalyst (0.16 wt %).

795 Noble metals such as Pt, Pd and Au were used as electrodes for the electrooxidation of  
796 hydrazine to N<sub>2</sub> and H<sub>2</sub> but their high price makes them not practical to use for further  
797 applications [119], [120]. Silver nano-catalysts Ag@C<sub>60</sub> were synthesised by Narwade et al.  
798 [121] to investigate the electrocatalytic activity for the oxidation of hydrazine for H<sub>2</sub>  
799 production. The electrocatalyst was also tested for its efficiency in a range of pH solutions. The  
800 best electrochemical performance and long-term stability was exhibited by the Ag@C<sub>60</sub>  
801 catalyst in a 0.5 M KOH solution. It was concluded that the enhanced electrocatalytic activity  
802 of the Ag@C<sub>60</sub> is a result of the synergistic effect of Ag nanoparticles and C<sub>60</sub>.

803 A new method studied recently is the photoelectrocatalysis, a combination of photocatalysis  
804 and electrocatalysis. Thus, photoelectrochemical (PEC) H<sub>2</sub> production from N<sub>2</sub>H<sub>4</sub>.H<sub>2</sub>O was  
805 studied by Yan et al. [122] using CdS nanorod arrays as the photoelectrode. The proposed  
806 mechanism is presented below in Fig.7. Under visible-light irradiation the photoelectrode in  
807 electrolytes with N<sub>2</sub>H<sub>4</sub>.H<sub>2</sub>O presented great stability after 100 h of the reaction while when  
808 there were no electrolytes the persistence of the device was less than 100 s. Moreover, the  
809 efficiency of the photoelectrode remained the same with a H<sub>2</sub> selectivity over 90%. The results  
810 that were obtained from the CdS photoelectrode promote the PEC H<sub>2</sub> production for further  
811 studies and applications. Table 4 summarises the results from the experiments mentioned  
812 above.



813 Fig.7. Proposed mechanism of the photoelectrochemical decomposition on CdS nanorod  
 814 catalysts [122].

815 Table 4. Photocatalysts and Electrocatalysts used for hydrous hydrazine decomposition.

Photocatalysis				
Catalyst	H <sub>2</sub> Yield (μmol)			Reference
Au/TiO <sub>2</sub>	48.5			[116]
Pd/SiO <sub>2</sub>	1.5			[117]
TiO <sub>2</sub> -Rh				[118]
Electrocatalysis				
Catalyst	System	Onset Potential	Current Density (mA cm <sup>-2</sup> )	Reference
Ni <sub>60</sub> Co <sub>40</sub>	1.0 M KOH + 0.1 M N <sub>2</sub> H <sub>4</sub> .H <sub>2</sub> O	1.56 V vs RHE		[119]
Ni/CB	0.1 M NaOH + 0.1 M N <sub>2</sub> H <sub>4</sub>	0.9245 V vs RHE		[120]
Ag@C <sub>60</sub>	0.5 M KOH + 0.5 mL N <sub>2</sub> H <sub>4</sub>	0.8 V vs SCE	112	[121]
Photoelectrocatalysis				
CdS NRs	0.1 M Na <sub>2</sub> SO <sub>4</sub> + 0.378 M N <sub>2</sub> H <sub>4</sub> .H <sub>2</sub> O	1.23 V vs RHE	7.6	[122]

816

## 817 **6 Reactors for NH<sub>3</sub> decomposition**

### 818 **6.1 Membrane reactors**

819 Catalytic membrane reactors (CMRs) are frequently used for the decomposition of ammonia  
820 because they offer several advantages. They shift the thermodynamic equilibrium due to the  
821 removal of H<sub>2</sub> allowing the process to proceed at lower temperatures reaching full conversion.  
822 Moreover, they do not require an additional separation unit, since separation and purification  
823 occur in a single unit, lowering the cost of the system and providing pure H<sub>2</sub>. The process is  
824 usually assisted by an inert sweep gas that might dilute H<sub>2</sub> stream, which is unwanted. The  
825 most suitable materials are Palladium or/and its alloys but their challenging scale-up and high  
826 cost limit this technology and therefore new materials must be explored [123].

827 Numerical simulations for ammonia decomposition in a catalytic membrane reactor filled with  
828 Ni/Al<sub>2</sub>O<sub>3</sub> catalytic particles were studied by Di Carlo et al [124]. The focus of the study was  
829 the evaluation of the improvement of the ammonia decomposition with the use of Pd coated  
830 membranes. Firstly, a 2D study was investigated without membranes and results showed that  
831 at temperature of 550°C, pressure of 0.2 MPa and low flow velocity of 2cm/s the ammonia  
832 conversion was extremely good with a residual NH<sub>3</sub> of only a few ppm. The 3D simulations  
833 were studied with the addition of Pd-membranes at 1MPa and temperature range of 500-600°C.  
834 At 550°C NH<sub>3</sub> conversion was 99.93% improving almost 18% the conversion rate that was  
835 obtained without the membranes.

836 A tube-wall catalytic membrane reactor containing a Pd membrane alloyed with Ag (Pd<sub>77</sub>Ag<sub>23</sub>)  
837 was developed by Itoh et al. [125] for the decomposition of ammonia at temperatures below  
838 400°C. A Ru catalyst was used, and the optimal loading was 2 wt% due to the high dispersion  
839 on the surface area. A 2 wt% Ru/Al<sub>2</sub>O<sub>3</sub> packed bed reactor was compared with the membrane  
840 reactor loaded with 2 wt% of Ru and it was found that the latter achieved a higher conversion  
841 (about 15% higher) because of the larger heat flux in the tube reactor. The reactor with 2 mm  
842 thick Pd membrane achieved 100% NH<sub>3</sub> conversion at 375°C and ammonia feed rate of 10  
843 mL/min.

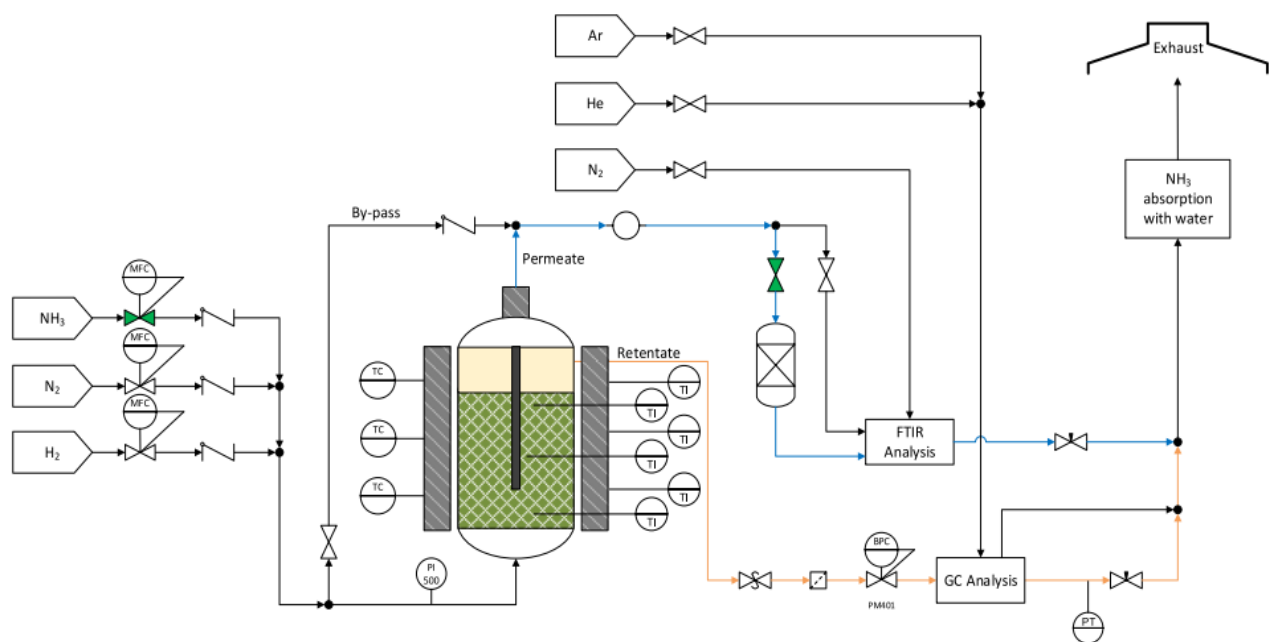
844 Abashar et al. [126] simulated multi-stage Pd-Ag membrane reactors for the generation of ultra-  
845 pure H<sub>2</sub>. In comparison with a single stage reactor that achieved 29.49 % ammonia conversion  
846 the seven-stage membrane reactor exhibited complete conversion of ammonia at 40 bar.

847 Moreover, a multi-stage fixed bed reactor was modelled under the same conditions and the exit  
848 ammonia conversion was 92.37% suggesting that a multi-stage membrane reactor is superior.  
849 The numerical results demonstrated a promising performance of the membrane reactor and  
850 even though they were not confirmed experimentally they might have fundamental importance  
851 for further design and optimization of the reactor and the process.

852 Co-based catalysts combined with Pd-Au alloy membranes were demonstrated by Cerrillo et  
853 al. [127] for the decomposition of ammonia to the production of high purity H<sub>2</sub>. Experiments  
854 were carried out with and without the addition of the membrane and results showed that the  
855 membrane drastically enhances the conversion of NH<sub>3</sub>. The purity of H<sub>2</sub> was > 99.97% for over  
856 1000 h of running stream. Moreover, the ammonia conversion increased when the temperature,  
857 pressure and contact time increased.

858 Cechetto et al. [128] experimentally demonstrated ammonia decomposition in a catalytic  
859 membrane reactor (Fig.8).The catalyst was Ru-based with double-skin Pd-based membranes.  
860 The main focus of the experiments was the purity of H<sub>2</sub> produced in the membrane reactor  
861 technology. Results showed that with an increase of the thickness of the membrane above 6  
862 μm ultra-pure H<sub>2</sub> can be generated. Also, a small purification unit can be installed as a more  
863 economic feasible solution in contrast with the increase of the membrane thickness. More  
864 specifically, a bed of 13X zeolite was tested and it was concluded that it's a suitable sorbent  
865 for H<sub>2</sub> purification.

866





867 Fig.8. Process flow diagram of the experimental setup [128].

868 In addition to that, membranes are required to be free of defects to achieve high H<sub>2</sub> purity.  
869 Alternative materials to Pd that have been already used are Vanadium, and Ni alloys. A 3D  
870 CFD model was developed by Shwe Hla and Dolan [129] for the examination of the  
871 performance of a Vanadium-based alloy membrane reactor for H<sub>2</sub> generation and separation  
872 by ammonia decomposition. At 30 L/min NH<sub>3</sub> inlet flow rate, pressure of 7.8 bar<sub>a</sub> and 300°C ,  
873 a conversion of 90 % NH<sub>3</sub> was achieved and H<sub>2</sub> yield over 95 % within a shorter distance along  
874 membrane tubes. As expected, at lower inlet flow rates, H<sub>2</sub> yield was higher due to a longer  
875 residence time. The effects of the membrane permeability on the H<sub>2</sub> yield were tested under  
876 different percentages of the original value. At only 50 % functionality the H<sub>2</sub> yield was similar  
877 with that obtained at 100 % membrane permeability.

878 A double layered Nd<sub>5.5</sub>Mo<sub>0.5</sub>W<sub>0.5</sub>O<sub>11.25-δ</sub> (NMW)/ Nd<sub>5.5</sub>Mo<sub>0.5</sub>W<sub>0.5</sub>O<sub>11.25-δ</sub>-Ni (NMW-Ni)  
879 membrane was synthesised by Cheng et al. [130] for the on-site H<sub>2</sub> production by catalytic  
880 ammonia decomposition. NMW-NiO layer served as the catalytic reaction site while the NMW  
881 layer provided the separation of H<sub>2</sub>. A sweep gas of N<sub>2</sub> was used and NH<sub>3</sub> conversion of 99 %  
882 was obtained at 750°C, 24% higher than that of a packed bed reactor that was achieved under  
883 the same conditions, given to the simultaneous removal of the H<sub>2</sub>. Moreover, the highest  
884 conversion may be attributed to the longer length of the membrane reactor. It was noticed that  
885 NH<sub>3</sub> conversion was higher at lower NH<sub>3</sub> flow rates in the feed stream due to a higher residence  
886 time of ammonia in the reactor, whereas H<sub>2</sub> production was small due to a slower composition  
887 rate, indicating the need to improve ammonia decomposition at high feed flow rates. After 75  
888 h of reaction at 750°C, the membrane reactor maintained a high conversion of 91 % achieving  
889 high long-term stability.

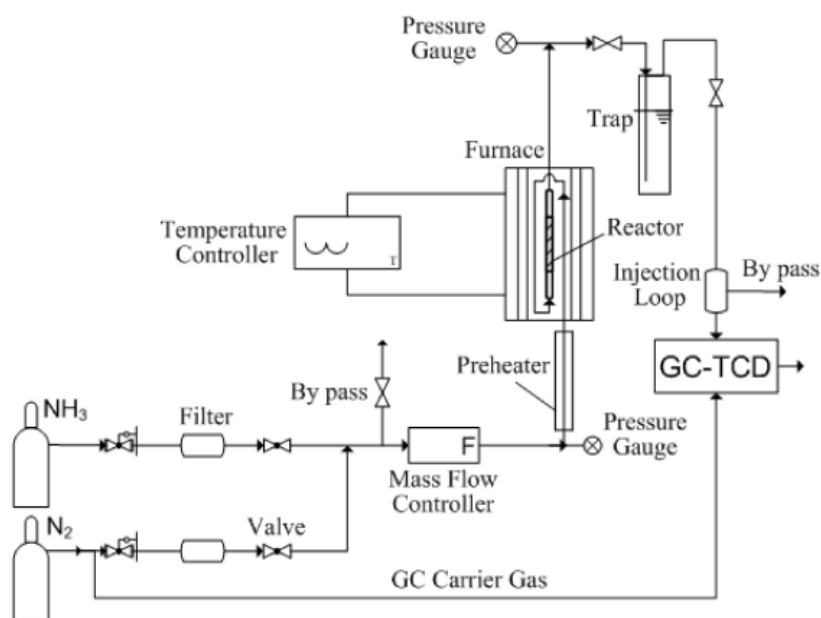
890 Ru particles dispersed on yttria-stabilized zirconium (YSZ) coated by a Pd film, were  
891 developed by Zhang et al. [131] to utilize them for H<sub>2</sub> production by the decomposition of NH<sub>3</sub>.  
892 The reaction took place in a catalytic membrane reactor. Different parameters such as  
893 temperature, pressure and inlet flow were tested to evaluate the reactor performance. An  
894 addition of Cs promoter caused complete decomposition of NH<sub>3</sub> at temperatures of 400°C and  
895 volumetric H<sub>2</sub> productivity of 31.6 mol m<sup>-3</sup> s<sup>-1</sup>. Both the catalyst and the membrane were found  
896 to eliminate any transport resistances resulting in a decreased operation temperature, reduced  
897 catalyst content and higher H<sub>2</sub> productivity in contrast with a PBMR. Also, a reactor model  
898 was developed to better understand the performance of the reactor. The experimental results

899 were in a great agreement with the model at all conditions, validating the first-order kinetics  
900 and the efficiency of the CMR.

## 901 **6.2 Fixed Bed Reactors**

902 Fixed bed reactors (FBRs) have many large-scale applications in the industry. One great  
903 advantage is that the catalyst is immobilized, and the reactant mixture is technically forced to  
904 be in contact with it. Though, due to its poor mixing properties large temperature gradients  
905 occur and therefore, the extent of the ammonia decomposition can be reduced [132].

906 Commercial 5 wt% Ru/C catalyst on different promoter Cs loadings was studied  
907 experimentally by Chen et al. [133] in a fixed bed reactor for the decomposition of ammonia.  
908 The experimental setup that was used in this work is demonstrated in Fig.9. The optimum  
909 Cs/Ru molar ratio was 4.5 and further increase than that resulted in a decrease on the conversion  
910 of ammonia. At 400°C ammonia conversion was nearly 100%.



920 Fig.9. Schematic diagram of the process for ammonia decomposition in a fixed bed reactor  
921 [133].

922 Gu et al. [134] developed Ni-based catalysts supported in porous alumina (Ni@Al<sub>2</sub>O<sub>3</sub>) via a  
923 simple one-pot method for the decomposition of ammonia. The Ni content was adjusted from  
924 5 at.% to 25 at.% and the reaction took place in a fixed bed reactor. The catalyst with the highest  
925 nickel content (25 at.%) exhibited the highest ammonia conversion of 93.9 % at 600°C and  
926 almost full conversion (99.1%) at 650°C. H<sub>2</sub> formation rate reached up to 7.8 mmol gcat<sup>-1</sup> min<sup>-1</sup>

927 <sup>1</sup> at 450°C. There was an increase in the crystallite size of Ni particles from 1 nm (fresh) to 6  
928 nm (used) due to high reaction temperature. The high catalytic performance could be attributed  
929 by the strong interaction amongst the mesoporous alumina matrix and nickel particles that can  
930 prevent the metallic Ni from sintering into large aggregates and the high dispersion of Ni  
931 particles.

932 A fixed bed plug flow reactor was used by Morlanés et al. [135] for the decomposition of  
933 ammonia by Ba-CoCe catalysts with various Co/Ce molar ratios. When catalysts were prepared  
934 by impregnation it was noticed that above 20 % of Co loading decreased the conversion of  
935 ammonia, while when they were prepared via coprecipitation the opposite trend was found  
936 since 30 % Co content catalysts showed higher activity. The high activity could be attributed  
937 to the coprecipitation method that allowed higher amounts of Co incorporated in the catalyst.  
938 The optimum performance was from the 0.5Ba/CoCe(80/20) catalyst with 41.4 wt % Co, 23.5  
939 wt % Ce and 0.45 wt % Ba, whose catalytic activity was comparable with Ru-based catalysts.  
940 At 450°C it exhibited a conversion little bit lower than 80 %. Ce as a promoter, increased Co  
941 dispersion and prevented sintering and aggregation.

942 Ru nanoparticles were supported on alkali silicates (Ru/A<sub>2</sub>SiO<sub>3</sub>, A = Li, Na and K) by Zhiqiang  
943 et al. [136] The catalytic reaction occurred in a fixed bed reactor at atmospheric pressure.  
944 Ru/K<sub>2</sub>SiO<sub>3</sub> (3.21 wt % Ru) showed the best catalytic performance with an NH<sub>3</sub> conversion of  
945 60.5 %, H<sub>2</sub> formation rate of 20.3 mmol g<sub>cat</sub><sup>-1</sup>min<sup>-1</sup> and TOF value of 2.03 s<sup>-1</sup> at 450°C. A series  
946 of K- promoted catalysts were prepared to evaluate the effect of the K content but results  
947 showed that the highest ammonia conversion was the one already exhibited by Ru/K<sub>2</sub>SiO<sub>3</sub>. In  
948 comparison with other works that used Ru particles supported on other silicon materials at the  
949 same conditions, Ru/K<sub>2</sub>SiO<sub>3</sub> achieved higher performance due to a better promotion effect of  
950 the alkali metal silicates. It was concluded by the authors that the formation of oxygen  
951 vacancies on the alkali metal silicates can stabilize the Ru nanoparticles with strong metal  
952 support interactions that results in an increase of the number of active sites.

953 Ni-Ru/CeO<sub>2</sub> catalysts with several metal loadings were prepared by Lucentini et al. [137] and  
954 tested for the H<sub>2</sub> generation from the decomposition of ammonia. The catalytic tests were  
955 carried in a fixed bed reactor and results showed that the best catalytic performance was  
956 observed by 0.4-0.6 wt% Ru and 2.4-5.0 wt% Ni. After 100 h of continuous operation the  
957 catalysts exhibited excellent long-term stability. At 400°C, TOF values exceeding 2 s<sup>-1</sup> were  
958 obtained. With the use of Langmuir-Hinshelwood-Hougen-Watson approach, a kinetic model

959 was developed for the simulation of the H<sub>2</sub> production rate under different parameters. Lastly,  
960 it was concluded that the limiting step for the reaction is the dehydrogenation of ammonia  
961 adsorbed on the surface of the catalysts.

962 In addition to the previous research Lucentini et al. [138] continued the investigation on the  
963 decomposition of ammonia on Ni-Ru catalysts supported on 3D-printed CeO<sub>2</sub> structures in a  
964 fixed bed reactor. The 0.5Ni0.1Ru catalyst achieved the best catalytic performance and  
965 therefore was used for the rest of the study. Moreover, a 1D mathematical model was developed  
966 over the 3D-printed catalytic structure loaded with Ni-Ru catalysts. A comparison between the  
967 experimental results and the simulation validated the model that was developed. For the  
968 optimisation of the catalytic structure, a series of simulations were performed with different  
969 geometric parameters to examine their effect on the catalytic performance in ammonia  
970 decomposition. Specifically, the geometric parameters that were optimized were the wall  
971 thickness, the number and width of channels for better and more efficient usage of the reactor  
972 with the intention of on-site generation H<sub>2</sub> and usage in a PEM-type fuel cell.

973 Co<sub>3</sub>Mo<sub>3</sub>N and  $\gamma$ -Mo<sub>2</sub>N catalysts were synthesised with the use of citric acid as a chelating agent  
974 by Jolaoso et al. [139]. The catalytic tests were performed in a fixed bed quartz tube reactor at  
975 atmospheric pressure, a temperature range of 300-600°C and constant GHSV of 6000 h<sup>-1</sup>. At  
976 550°C,  $\gamma$ -Mo<sub>2</sub>N catalyst gave 71.9 % NH<sub>3</sub> conversion while Co<sub>3</sub>Mo<sub>3</sub>N gave 97.3 % resulting  
977 in a better catalytic performance indicating that Co particles promote the ammonia  
978 decomposition. Characterization tests showed that Co<sub>3</sub>Mo<sub>3</sub>N catalyst contained 33.72 wt %,   
979 54.41 wt % and 4.03 wt % Co, Mo and N respectively. After 35 h of a continuous test the  
980 catalyst showed no deactivation. This was validated by measuring the crystallite size of the  
981 fresh catalyst (6.20 nm) and the used catalyst (6.19 nm) whereas no significant decrease was  
982 obtained. Conversion of 100 % was obtained by both catalysts at 600°C.

983 Another study conducted in a fixed bed reactor, implemented three Ru-supported catalysts  
984 (Ru/Al<sub>2</sub>O<sub>3</sub>, Ru/La<sub>2</sub>O<sub>3</sub>-Al<sub>2</sub>O<sub>3</sub> and Ru/La<sub>2</sub>O<sub>2</sub>CO<sub>3</sub>-Al<sub>2</sub>O<sub>3</sub>). Kim et al. [140] examined their  
985 catalytic activity at a low temperature range of 350-500°C. The best catalytic activity was  
986 established by Ru/La<sub>2</sub>O<sub>2</sub>CO<sub>3</sub>-Al<sub>2</sub>O<sub>3</sub> (11.5 wt % La and 0.95 wt % Ru) with 80.1 % NH<sub>3</sub>  
987 conversion at 500°C. Even though characterization tests showed that Ru/Al<sub>2</sub>O<sub>3</sub> had higher Ru  
988 dispersion (27.3 %) than Ru/La<sub>2</sub>O<sub>3</sub>-Al<sub>2</sub>O<sub>3</sub> (20.6 %) it resulted in a lower catalytic activity  
989 suggesting that the La addition promoted electron donation from La to Ru particles due to their  
990 electronegativity difference and therefore increasing the kinetics of the reaction. Moreover, the

991 La oxycarbonate-rich surface favoured the formation of Ru particles on the surface of the  
992 catalyst preventing the particles to leave from the surface into the bulk phase. Thus, it was  
993 concluded that the  $\text{La}_2\text{O}_2\text{CO}_3$  surface coating might be beneficial for catalyst synthesis when  
994 an increased surface metal concentration is needed.

### 995 **6.3 Microreactors**

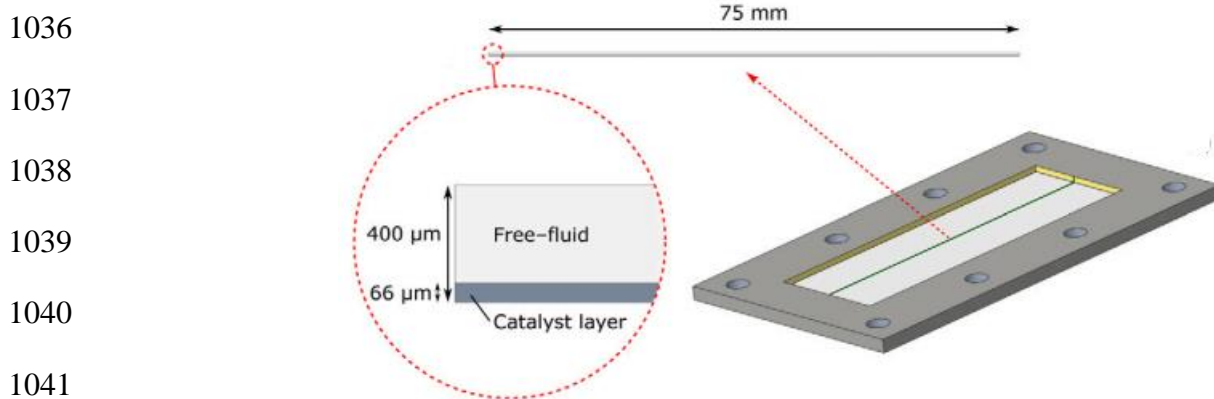
996 Microreactors gained attention in the early 1990s marking them as a relatively new field.  
997 Microreactor technology offers better control, high surface area ratios, high heat and mass  
998 transfer rates and enhanced conversion efficiency. Compared with conventional reactors, micro  
999 structured reactors exhibited higher activity towards  $\text{NH}_3$  ammonia decomposition [141].

1000 An autothermal microchannel reactor was evaluated for the decomposition of ammonia to  
1001 generate  $\text{H}_2$  and provide it for power generation systems. Engelbrecht, Chiuta and Bessarabov  
1002 [142] studied the effects of different parameters such as  $\text{NH}_3$  decomposition flow rate and  
1003 oxidation flow rate and fuel-oxygen equivalence ratio to find the optimal operation parameters.  
1004 The catalyst for decomposition was 8.5 wt%  $\text{Ru}/\text{Al}_2\text{O}_3$  and for the oxidation was 5 wt%  
1005  $\text{Pt}/\text{Al}_2\text{O}_3$ . A conversion up to 99.8% was observed with a  $\text{H}_2$  equivalent fuel power of 0.71  
1006  $\text{kWe}$ , when the decomposition flow rate was 6  $\text{NL min}^{-1}$ , the oxidation flow rate was 4  $\text{NL}$   
1007  $\text{min}^{-1}$  and the fuel-oxygen ratio was 1.4. A stability test was also carried out for 24 h in  
1008 demanding reactor conditions to determine any inconsistencies in the catalyst where results  
1009 showed that no deactivation of the catalyst occurred during reaction. It was concluded that the  
1010 performance of the reactor was good and further research might be able to up-scale this system  
1011 for multi-kW power generation systems.

1012 Based on the experimental results obtained from Engelbrecht, Chiuta and Bessarabov [142], a  
1013 3D CFD model was developed by Schumacher et al. [143] to study both steady-state and  
1014 transient regimes in a microchannel reactor to provide a suitable mathematical model. In  
1015 consideration of the wide range of ammonia decomposition and oxidation flow rates and  
1016 temperature profiles, the simulation fitted the experimental data with an acceptable accuracy.  
1017 It was found that at the microreactor inlet the highest temperature was obtained and therefore  
1018 a different solution needed to be developed to solve the model with regard in the distribution  
1019 of heat transfer. Therefore, any future reactor designs should be focused on the optimization of  
1020 the heat transfer rate.

1021 3D printed SiCN monolithic ceramic microreactors and Ru catalysts were used by Gyak et al.  
1022 [144] for ammonia decomposition at high temperature. A temperature range of 500-1000°C  
1023 and different flow rates of 2, 4 and 8 mL min<sup>-1</sup> were the conditions for the catalytic reaction.  
1024 At 2 mL min<sup>-1</sup> and 1000°C, ammonia was completely decomposed due to an increased  
1025 residence time. After 48 h of exposure to ammonia and 1000°C, the ceramic microreactors  
1026 demonstrated excellent chemical resistance and heat tolerance.

1027 Maleki, Fulton and Bertola [145] designed a microreactor, both experimentally and  
1028 numerically for H<sub>2</sub> production via low temperature ammonia decomposition over  
1029 Co<sub>0.5</sub>Ce<sub>0.1</sub>Al<sub>0.4</sub>O(sa) catalyst. The geometries of the microchannel are presented in Fig.10. Two  
1030 kinetic models were used to describe the reaction, a pseudo-first order model and a modified  
1031 Temkin-Pyzhev model that were compiled in a CFD model. The model then was solved at a  
1032 various NH<sub>3</sub> flow rates and temperatures and exhibited good agreement with the experimental  
1033 data. At a lower temperature range the Temkin-Pyzhev model had better accuracy than the first  
1034 model and therefore was selected for further study. Higher conversion rates were obtained  
1035 while increasing the temperatures whereas over 99 % was observed at temperatures of 550°C.



1042 Fig.10. 2D and 3D geometries of the microreactor [145].

1043 Bimetallic Ru-Fe alloy catalysts were synthesised and impregnated with carbon nanotubes by  
1044 Chen et al. [146] The experiments took place in a fixed bed microreactor at a temperature range  
1045 of 300-500°C and atmospheric pressure. The Ru<sub>3</sub>Fe/CNTs catalyst (1.67 wt % Ru, 0.31 wt %  
1046 Fe) presented the best catalytic performance in contrast with the Ru/CNTs catalyst. At 500°C  
1047 both catalysts resulted in a 100 % ammonia conversion. After 60 h of reaction, the activity of  
1048 Ru/CNTs was decreased by 30 % while that of Ru<sub>3</sub>Fe/CNTs decreased only 10 % exhibiting  
1049 superior stability with the addition of Ru. It was concluded that the alloy synergistic effect

1050 between Ru and Fe enhanced the catalytic activity and furthermore the addition of the non-  
 1051 noble metal Fe reduces the content of Ru resulting in a lower catalyst cost.

1052 Table 5. A summary of the type of reactors used for ammonia decomposition

Type of reactor	Catalyst	Temperature	Conversion	Yield	TOF	Reference
Pd membrane reactor	Ni/Al <sub>2</sub> O <sub>3</sub>	550	99.93			[124]
Pd membrane reactor	2%Ru/Al <sub>2</sub> O <sub>3</sub>	375	100			[125]
Pd-Ag membrane reactor			100			[126]
Pd-Au membrane reactor	Co			99.97		[127]
Double-skin Pd membrane reactor	Ru			93.2		[128]
Vanadium alloy membrane reactor		300	90	>95		[129]
NMW/NMW-NiO	NMW-NiO powder	750	99			[130]
YSZ/Pd membrane reactor	Ru	400	93	90		[131]
Fixed bed reactor	5%Ru/C	400	~100			[133]
Fixed bed reactor	25%Ni@Al <sub>2</sub> O <sub>3</sub>	650	99.1			[134]
Fixed bed reactor	0.5Ba/CoCe(80/20)	450	74		0.602	[135]
Fixed bed reactor	Ru/K <sub>2</sub> SiO <sub>3</sub>	450	60.5		2.03	[136]
Fixed bed reactor	Ni-Ru/CeO <sub>2</sub>	400			2	[137]
Fixed bed reactor	Ni-Ru/CeO <sub>2</sub>					[138]
Fixed bed reactor	Co <sub>3</sub> Mo <sub>3</sub> N	550	97.3			[139]
Fixed bed reactor	Ru/La <sub>2</sub> O <sub>2</sub> CO <sub>3</sub> -Al <sub>2</sub> O <sub>3</sub>	500	80.1			[140]
Microreactor	8.5%Ru/Al <sub>2</sub> O <sub>3</sub>	651	99.8			[142]
Microreactor – Experimental	Ru/Al <sub>2</sub> O <sub>3</sub>	300	99.86			[143]
Microreactor – Simulation	Ru/Al <sub>2</sub> O <sub>3</sub>	300	99.94			[143]
Microreactor	Ru	1000	100			[144]
Microreactor	Co <sub>0.5</sub> Ce <sub>0.1</sub> Al <sub>0.4</sub> O(sa)	550	99			[145]
Microreactor	Ru <sub>3</sub> Fe/CNTs	500	100		86.21	[146]

1053 As seen from Table 5 membrane reactors and microreactors are superior to fixed bed reactors.  
 1054 Even though membrane reactors are well studied, the most common membrane used is Pd and  
 1055 its alloys [124]–[128], [131], which is rare and expensive and needs to be replaced with other  
 1056 elements that give off such high catalytic activity and selectivity. Regarding fixed bed reactors,  
 1057 a number of studies give promising results but most of them presented low conversion of  
 1058 ammonia [135]–[137], [140]. The need for high temperatures for the decomposition makes  
 1059 these reactors unsuitable. Studies on microreactors operating experimentally and theoretically

1060 in a large range of temperatures are limited mostly for Ru-based catalysts as they present high  
1061 catalytic activity giving the opportunity for further development of a cost-effective reactor  
1062 system [143], [144], [146].

1063

## 1064 **7 Conclusions**

1065 Green energy carriers have the potential to solve the current issues related with climate change.  
1066 An emerging energy resource is H<sub>2</sub> as an alternative to non-renewable sources such as  
1067 conventional fuels. Its physical storage though, is limiting its application. Therefore, this  
1068 review provides information about ammonia and hydrous hydrazine as possible chemical  
1069 hydrogen storage compounds. Moreover, heterogeneous catalysts utilized for the  
1070 decomposition reactions of the compounds mentioned above are reviewed in contrast with their  
1071 efficiency. An issue occurring with hydrous hydrazine decomposition is ammonia formation  
1072 that can lead to corrosion and lower selectivity regarding H<sub>2</sub>. The most promising catalytic  
1073 system for ammonia decomposition is ruthenium and its alloys but it's not methodical due to  
1074 its high price and scarcity. For hydrous hydrazine, the most active catalytic system is nickel  
1075 catalysts alloyed with noble metals that are some of the most expensive metals in the world.  
1076 Thus, there is a great need for the development of cost-effective catalytic systems for both  
1077 ammonia and hydrous hydrazine, using more abundant metals instead of precious metals with  
1078 lower metal loading and higher atom efficiency. Reactor technology used for NH<sub>3</sub>  
1079 decomposition has also been presented in this review. The most common catalyst used for this  
1080 reaction is the catalytic membrane reactor. Due to the membrane, separation and purification  
1081 can occur in a single step, giving pure H<sub>2</sub> and lowering the operation cost. Palladium  
1082 membranes were found to be the most suitable materials, but future works need to take into  
1083 consideration their high cost and therefore, explore and develop other materials with the same  
1084 efficacy. Microreactors are also an attractive option due to a high activity towards NH<sub>3</sub> with  
1085 different types of catalysts, especially ruthenium and its alloys. In contrast, fixed bed reactors  
1086 presented lower activity and further research is needed for future applications and up-scaled  
1087 production of H<sub>2</sub>. In conclusion, for on-site hydrogen production by NH<sub>3</sub> and N<sub>2</sub>H<sub>4</sub>.H<sub>2</sub>O future  
1088 research must give attention to the development of low-cost catalyst with optimum catalytic  
1089 performance and great selectivity towards H<sub>2</sub>. Furthermore, it's important to consider the  
1090 reactor technology and develop systems with low operation cost and high efficiency.



1091

## 1092 **References**

- 1093 [1] K. Mazloomi and C. Gomes, “Hydrogen as an energy carrier: Prospects and  
1094 challenges,” *Renew. Sustain. Energy Rev.*, vol. 16, no. 5, pp. 3024–3033, Jun. 2012,  
1095 doi: 10.1016/J.RSER.2012.02.028.
- 1096 [2] A. Pareek, R. Dom, J. Gupta, J. Chandran, V. Adepur, and P. H. Borse, “Insights into  
1097 renewable hydrogen energy: Recent advances and prospects,” *Mater. Sci. Energy  
1098 Technol.*, vol. 3, pp. 319–327, Jan. 2020, doi: 10.1016/J.MSET.2019.12.002.
- 1099 [3] S. Shiva Kumar and V. Himabindu, “Hydrogen production by PEM water electrolysis  
1100 – A review,” *Mater. Sci. Energy Technol.*, vol. 2, no. 3, pp. 442–454, Dec. 2019, doi:  
1101 10.1016/J.MSET.2019.03.002.
- 1102 [4] S. Atilhan, S. Park, M. M. El-Halwagi, M. Atilhan, M. Moore, and R. B. Nielsen,  
1103 “Green hydrogen as an alternative fuel for the shipping industry,” *Curr. Opin. Chem.  
1104 Eng.*, vol. 31, Mar. 2021, doi: 10.1016/J.COCHE.2020.100668.
- 1105 [5] M. Ji and J. Wang, “Review and comparison of various hydrogen production methods  
1106 based on costs and life cycle impact assessment indicators,” *Int. J. Hydrogen Energy*,  
1107 vol. 46, no. 78, pp. 38612–38635, Nov. 2021, doi: 10.1016/J.IJHYDENE.2021.09.142.
- 1108 [6] K. Scott, “Chapter 1 Introduction to Electrolysis, Electrolysers and Hydrogen  
1109 Production,” *RSC Energy Environ. Ser.*, vol. 2020-January, no. 25, pp. 1–27, 2019,  
1110 doi: 10.1039/9781788016049-00001.
- 1111 [7] R. A. Felseghi, E. Carcadea, M. S. Raboaca, C. N. Trufin, and C. Filote, “Hydrogen  
1112 Fuel Cell Technology for the Sustainable Future of Stationary Applications,” *Energies  
1113 2019, Vol. 12, Page 4593*, vol. 12, no. 23, p. 4593, Dec. 2019, doi:  
1114 10.3390/EN12234593.
- 1115 [8] S. Zhang, Z. He, X. Li, J. Zhang, Q. Zang, and S. Wang, “Building heterogeneous  
1116 nanostructures for photocatalytic ammonia decomposition,” *Nanoscale Adv.*, vol. 2,  
1117 no. 9, pp. 3610–3623, 2020, doi: 10.1039/d0na00161a.
- 1118 [9] Y. Kojima, “Hydrogen storage materials for hydrogen and energy carriers,” *Int. J.  
1119 Hydrogen Energy*, vol. 44, no. 33, pp. 18179–18192, 2019, doi:  
1120 10.1016/j.ijhydene.2019.05.119.

- 1121 [10] M. Aziz, A. TriWijayanta, and A. B. D. Nandiyanto, "Ammonia as effective hydrogen  
1122 storage: A review on production, storage and utilization," *Energies*, vol. 13, no. 12, pp.  
1123 1–25, 2020, doi: 10.3390/en13123062.
- 1124 [11] M. J. Palys and P. Daoutidis, "Using hydrogen and ammonia for renewable energy  
1125 storage: A geographically comprehensive techno-economic study," *Comput. Chem.  
1126 Eng.*, vol. 136, p. 106785, 2020, doi: 10.1016/j.compchemeng.2020.106785.
- 1127 [12] M. Tawalbeh, S. Z. M. Murtaza, A. Al-Othman, A. H. Alami, K. Singh, and A. G.  
1128 Olabi, "Ammonia: A versatile candidate for the use in energy storage systems,"  
1129 *Renew. Energy*, vol. 194, pp. 955–977, 2022, doi: 10.1016/j.renene.2022.06.015.
- 1130 [13] K. E. Lamb, M. D. Dolan, and D. F. Kennedy, "Ammonia for hydrogen storage; A  
1131 review of catalytic ammonia decomposition and hydrogen separation and purification,"  
1132 *Int. J. Hydrogen Energy*, vol. 44, no. 7, pp. 3580–3593, 2019, doi:  
1133 10.1016/j.ijhydene.2018.12.024.
- 1134 [14] W. Ramsay and S. Young, "The decomposition of ammonia by heat," no. 88, pp. 88–  
1135 93, 1884.
- 1136 [15] E. P. Perman and G. A. S. Atkinson, "The decomposition of ammonia by heat," vol.  
1137 44, pp. 110–117, 1904.
- 1138 [16] B. Robert Matt air, H. H. Sisler, F. Raschig, and V. Chemie GmbH, "Hydrazine from  
1139 Chlorine with Anhydrous Ammonia The Production of Hydrazine by the Reaction of  
1140 Chlorine with Anhydrous Ammonia1."
- 1141 [17] S. Zhong and Q. Xu, "Metal nanoparticle-catalyzed hydrogen generation from liquid  
1142 chemical hydrides," *Bull. Chem. Soc. Jpn.*, vol. 91, no. 11, pp. 1606–1617, 2018, doi:  
1143 10.1246/bcsj.20180227.
- 1144 [18] D. X. Zhang, H. Yin, H. F. Zhong, L. Y. Gan, and P. Wang, "Linear scaling relations  
1145 for N<sub>2</sub>H<sub>4</sub> decomposition over transition metal catalysts," *Int. J. Hydrogen Energy*, vol.  
1146 45, no. 32, pp. 16114–16121, 2020, doi: 10.1016/j.ijhydene.2020.04.054.
- 1147 [19] S. Prabu, M. Vinu, and K. Y. Chiang, "Metal nanoparticles supported on crystalline  
1148 Al(OH)<sub>3</sub> Nano sheets for efficient catalytic hydrogen production from hydrous  
1149 hydrazine in aqueous solution," *Int. J. Energy Res.*, vol. 45, no. 13, pp. 18857–18874,  
1150 2021, doi: 10.1002/er.6975.

- 1151 [20] V. A. Matyshak and O. N. Silchenkova, “Catalytic Decomposition of Hydrazine and  
1152 Hydrazine Derivatives to Produce Hydrogen-Containing Gas Mixtures: A Review,”  
1153 *Kinet. Catal.*, vol. 63, no. 4, pp. 339–350, 2022, doi: 10.1134/s0023158422040073.
- 1154 [21] L. Zhou, X. Luo, L. Xu, C. Wan, and M. Ye, “Pt-Ni nanoalloys for H<sub>2</sub> generation from  
1155 Hydrous Hydrazine,” *Catalysts*, vol. 10, no. 8, 2020, doi: 10.3390/catal10080930.
- 1156 [22] R. Tarkowski, “Underground hydrogen storage: Characteristics and prospects,” *Renew.*  
1157 *Sustain. Energy Rev.*, vol. 105, no. January, pp. 86–94, 2019, doi:  
1158 10.1016/j.rser.2019.01.051.
- 1159 [23] Alexander Körner, “Technology Roadmap Hydrogen and Fuel Cells,” 2015.
- 1160 [24] J. Zheng, X. Liu, P. Xu, P. Liu, Y. Zhao, and J. Yang, “Development of high pressure  
1161 gaseous hydrogen storage technologies,” *Int. J. Hydrogen Energy*, vol. 37, no. 1, pp.  
1162 1048–1057, Jan. 2012, doi: 10.1016/J.IJHYDENE.2011.02.125.
- 1163 [25] E. Rivard, M. Trudeau, and K. Zaghib, “Hydrogen storage for mobility: A review,”  
1164 *Materials (Basel)*., vol. 12, no. 12, 2019, doi: 10.3390/ma12121973.
- 1165 [26] Z. Free, M. Hernandez, M. Mashal, and K. Mondal, “A review on advanced  
1166 manufacturing for hydrogen storage applications,” *Energies*, vol. 14, no. 24, 2021, doi:  
1167 10.3390/en14248513.
- 1168 [27] D. P. Broom and M. Hirscher, “Irreproducibility in hydrogen storage material  
1169 research,” *Energy Environ. Sci.*, vol. 9, no. 11, pp. 3368–3380, 2016, doi:  
1170 10.1039/c6ee01435f.
- 1171 [28] A. C. Dillon, K. M. Jones, T. A. Bekkedahl, C. H. Kiang, D. S. Bethune, and M. J.  
1172 Heben, “Storage of hydrogen in single-walled carbon nanotubes,” *Nature*, vol. 386. pp.  
1173 377–379, 1997.
- 1174 [29] A. Chambers, C. Park, R. Terry, K. Baker, and N. M. Rodriguez, “Hydrogen Storage  
1175 in Graphite Nanofibers,” vol. 102, 1998.
- 1176 [30] M. Becher *et al.*, “Hydrogen storage in carbon nanotubes,” *Comptes Rendus Phys.*,  
1177 vol. 4, no. 9, pp. 1055–1062, 2003, doi: 10.1016/S1631-0705(03)00107-5.
- 1178 [31] G. G. Tibbetts, G. P. Meisner, and C. H. Olk, “Hydrogen storage capacity of carbon  
1179 nanotubes, filaments, and vapor-grown fibers,” *Carbon N. Y.*, vol. 39, no. 15, pp.  
1180 2291–2301, 2001, doi: 10.1016/S0008-6223(01)00051-3.

- 1181 [32] M. Rzepka *et al.*, “Hydrogen Storage Capacity of Catalytically Grown Carbon  
1182 Nanofibers,” 2005, doi: 10.1021/jp051371a.
- 1183 [33] S. Liu, L. Guo, H. Jin, L. Li, G. Li, and L. Yu, “Hydrogen production by supercritical  
1184 water gasification of coal: A reaction kinetic model including nitrogen and sulfur  
1185 elements,” *Int. J. Hydrogen Energy*, vol. 45, no. 56, pp. 31732–31744, Nov. 2020, doi:  
1186 10.1016/J.IJHYDENE.2020.08.166.
- 1187 [34] S. I. Ngo, Y. Il Lim, W. Kim, D. J. Seo, and W. L. Yoon, “Computational fluid  
1188 dynamics and experimental validation of a compact steam methane reformer for  
1189 hydrogen production from natural gas,” *Appl. Energy*, vol. 236, pp. 340–353, Feb.  
1190 2019, doi: 10.1016/J.APENERGY.2018.11.075.
- 1191 [35] H. H. Cho, V. Strezov, and T. J. Evans, “Environmental impact assessment of  
1192 hydrogen production via steam methane reforming based on emissions data,” *Energy  
1193 Reports*, vol. 8, pp. 13585–13595, Nov. 2022, doi: 10.1016/J.EGYR.2022.10.053.
- 1194 [36] M. H. Ali Khan, R. Daiyan, P. Neal, N. Haque, I. MacGill, and R. Amal, “A  
1195 framework for assessing economics of blue hydrogen production from steam methane  
1196 reforming using carbon capture storage & utilisation,” *Int. J. Hydrogen Energy*, vol.  
1197 46, no. 44, pp. 22685–22706, Jun. 2021, doi: 10.1016/J.IJHYDENE.2021.04.104.
- 1198 [37] M. Yu, K. Wang, and H. Vredenburg, “Insights into low-carbon hydrogen production  
1199 methods: Green, blue and aqua hydrogen,” *Int. J. Hydrogen Energy*, vol. 46, no. 41,  
1200 pp. 21261–21273, Jun. 2021, doi: 10.1016/J.IJHYDENE.2021.04.016.
- 1201 [38] J. Chi and H. Yu, “Water electrolysis based on renewable energy for hydrogen  
1202 production,” *Cuihua Xuebao/Chinese J. Catal.*, vol. 39, no. 3, pp. 390–394, Mar. 2018,  
1203 doi: 10.1016/S1872-2067(17)62949-8.
- 1204 [39] M. Hermesmann and T. E. Müller, “Green, Turquoise, Blue, or Grey? Environmentally  
1205 friendly Hydrogen Production in Transforming Energy Systems,” *Prog. Energy  
1206 Combust. Sci.*, vol. 90, May 2022, doi: 10.1016/J.PECS.2022.100996.
- 1207 [40] F. Dawood, M. Anda, and G. M. Shafiullah, “Hydrogen production for energy: An  
1208 overview,” *Int. J. Hydrogen Energy*, vol. 45, no. 7, pp. 3847–3869, Feb. 2020, doi:  
1209 10.1016/J.IJHYDENE.2019.12.059.
- 1210 [41] A. E. Karaca, I. Dincer, and J. Gu, “Life cycle assessment study on nuclear based

- 1211 sustainable hydrogen production options,” *Int. J. Hydrogen Energy*, vol. 45, no. 41, pp.  
1212 22148–22159, Aug. 2020, doi: 10.1016/J.IJHYDENE.2020.06.030.
- 1213 [42] S. E. Hosseini and M. A. Wahid, “Hydrogen from solar energy, a clean energy carrier  
1214 from a sustainable source of energy,” *Int. J. Energy Res.*, vol. 44, no. 6, pp. 4110–  
1215 4131, 2020, doi: 10.1002/er.4930.
- 1216 [43] A. Boretti, “There are hydrogen production pathways with better than green hydrogen  
1217 economic and environmental costs,” *Int. J. Hydrogen Energy*, vol. 46, no. 46, pp.  
1218 23988–23995, Jul. 2021, doi: 10.1016/J.IJHYDENE.2021.04.182.
- 1219 [44] M. Noussan, P. P. Raimondi, R. Scita, and M. Hafner, “The role of green and blue  
1220 hydrogen in the energy transition—a technological and geopolitical perspective,”  
1221 *Sustain.*, vol. 13, no. 1, pp. 1–26, 2021, doi: 10.3390/su13010298.
- 1222 [45] G. Baskar, R. Aiswarya, S. Soumiya, N. Mohanapriya, and S. Roselin Nivetha,  
1223 “Recent Advances in Heterogeneous Catalysts for Biodiesel Production,” *J. Energy*  
1224 *Environ. Sustain.*, vol. 4, pp. 1–5, Jul. 2017, doi: 10.47469/JEES.2017.V04.100038.
- 1225 [46] D. J. Richardson, K. Hellgardt, P. A. Russell, G. Mason, and B. A. Buffman, “Flux  
1226 Response Analysis: A Study of Ammonia Decomposition Over Pt/Alumina,” *Chem.*  
1227 *Eng. Res. Des.*, vol. 82, no. 10, pp. 1397–1403, Oct. 2004, doi:  
1228 10.1205/CERD.82.10.1397.46741.
- 1229 [47] J. Polanski *et al.*, “Ni-Supported Pd Nanoparticles with Ca Promoter: A New Catalyst  
1230 for Low-Temperature Ammonia Cracking,” *PLoS One*, vol. 10, no. 8, p. e0136805,  
1231 Aug. 2015, doi: 10.1371/JOURNAL.PONE.0136805.
- 1232 [48] C. Huang *et al.*, “Ru/La<sub>2</sub>O<sub>3</sub> catalyst for ammonia decomposition to hydrogen,”  
1233 *Appl. Surf. Sci.*, vol. 476, no. November 2018, pp. 928–936, 2019, doi:  
1234 10.1016/j.apsusc.2019.01.112.
- 1235 [49] C. Popa, W. K. Offermans, R. A. Van Santen, and A. P. J. Jansen, “Ab initio density-  
1236 functional theory study of NH<sub>x</sub> dehydrogenation and reverse reactions on the Rh(111)  
1237 surface,” doi: 10.1103/PhysRevB.74.155428.
- 1238 [50] S. Mukherjee, S. V. Devaguptapu, A. Sviripa, C. R. F. Lund, and G. Wu, “Low-  
1239 temperature ammonia decomposition catalysts for hydrogen generation,” *Appl. Catal.*  
1240 *B Environ.*, vol. 226, no. August 2017, pp. 162–181, 2018, doi:

- 1241 10.1016/j.apcatb.2017.12.039.
- 1242 [51] S. F. Yin, B. Q. Xu, X. P. Zhou, and C. T. Au, “A mini-review on ammonia  
1243 decomposition catalysts for on-site generation of hydrogen for fuel cell applications,”  
1244 *Appl. Catal. A Gen.*, vol. 277, no. 1–2, pp. 1–9, 2004, doi:  
1245 10.1016/j.apcata.2004.09.020.
- 1246 [52] B. Lorenzut *et al.*, “Embedded Ru@ZrO<sub>2</sub> Catalysts for H<sub>2</sub> Production by Ammonia  
1247 Decomposition,” vol. 2, no. 9, pp. 1096–1106, 2010, doi: 10.1002/cctc.201000097.
- 1248 [53] A. Takahashi and T. Fujitani, “Kinetic Analysis of Decomposition of Ammonia over  
1249 Nickel and Ruthenium Catalysts,” *J. Chem. Eng. Japan*, vol. 49, no. 1, pp. 22–28,  
1250 2016, doi: 10.1252/jcej.14we431.
- 1251 [54] X. Ju *et al.*, “Mesoporous Ru/MgO prepared by a deposition-precipitation method as  
1252 highly active catalyst for producing CO<sub>x</sub>-free hydrogen from ammonia  
1253 decomposition,” *Appl. Catal. B Environ.*, vol. 211, pp. 167–175, 2017, doi:  
1254 10.1016/j.apcatb.2017.04.043.
- 1255 [55] C. Chen *et al.*, “Ru-Based Catalysts for Ammonia Decomposition: A Mini-Review,”  
1256 *Energy and Fuels*, vol. 35, no. 15, pp. 11693–11706, 2021, doi:  
1257 10.1021/acs.energyfuels.1c01261.
- 1258 [56] Y. Qiu, E. Fu, F. Gong, and R. Xiao, “Catalyst support effect on ammonia  
1259 decomposition over Ni/MgAl<sub>2</sub>O<sub>4</sub> towards hydrogen production,” *Int. J. Hydrogen  
1260 Energy*, vol. 47, no. 8, pp. 5044–5052, 2022, doi: 10.1016/j.ijhydene.2021.11.117.
- 1261 [57] G. Li, H. Zhang, X. Yu, Z. Lei, F. Yin, and X. He, “Highly efficient Co/NC catalyst  
1262 derived from ZIF-67 for hydrogen generation through ammonia decomposition,” *Int. J.  
1263 Hydrogen Energy*, vol. 47, no. 26, pp. 12882–12892, 2022, doi:  
1264 10.1016/j.ijhydene.2022.02.046.
- 1265 [58] H. Tang *et al.*, “Catalytic activity of Ru supported on SmCeO<sub>x</sub> for ammonia  
1266 decomposition: The effect of Sm doping,” *J. Solid State Chem.*, vol. 295, no. October  
1267 2020, p. 121946, 2021, doi: 10.1016/j.jssc.2020.121946.
- 1268 [59] G. Li, X. Yu, F. Yin, Z. Lei, H. Zhang, and X. He, “Production of hydrogen by  
1269 ammonia decomposition over supported Co<sub>3</sub>O<sub>4</sub> catalysts,” *Catal. Today*, vol. 402, no.  
1270 November 2021, pp. 45–51, 2022, doi: 10.1016/j.cattod.2022.02.020.

- 1271 [60] M. Pinzón, O. Avilés-García, A. R. de la Osa, A. de Lucas-Consuegra, P. Sánchez, and  
1272 A. Romero, “New catalysts based on reduced graphene oxide for hydrogen production  
1273 from ammonia decomposition,” *Sustain. Chem. Pharm.*, vol. 25, no. January, 2022,  
1274 doi: 10.1016/j.scp.2022.100615.
- 1275 [61] K. G. Kirste *et al.*, “CO<sub>x</sub>-free hydrogen production from ammonia – mimicking the  
1276 activity of Ru catalysts with unsupported Co-Re alloys,” *Appl. Catal. B Environ.*, vol.  
1277 280, no. August 2020, p. 119405, 2021, doi: 10.1016/j.apcatb.2020.119405.
- 1278 [62] A. Jedynak, Z. Kowalczyk, D. Szmigiel, W. Raróg, and J. Zieliński, “Ammonia  
1279 decomposition over the carbon-based iron catalyst promoted with potassium,” *Appl.*  
1280 *Catal. A Gen.*, vol. 237, no. 1–2, pp. 223–226, 2002, doi: 10.1016/S0926-  
1281 860X(02)00330-7.
- 1282 [63] J. C. Ganley, F. S. Thomas, E. G. Seebauer, and R. I. Masel, “A priori catalytic activity  
1283 correlations: The difficult case of hydrogen production from ammonia,” *Catal. Letters*,  
1284 vol. 96, no. 3–4, pp. 117–122, 2004, doi: 10.1023/B:CATL.0000030108.50691.d4.
- 1285 [64] J. Zhang, M. Comotti, F. Schüth, R. Schlögl, and D. S. Su, “Commercial Fe- or Co-  
1286 containing carbon nanotubes as catalysts for NH<sub>3</sub> decomposition,” *Chem. Commun.*,  
1287 no. 19, pp. 1916–1918, 2007, doi: 10.1039/b700969k.
- 1288 [65] M. El-Shafie, S. Kambara, and Y. Hayakawa, “Development of zeolite-based catalyst  
1289 for enhancement hydrogen production from ammonia decomposition,” *Catal. Today*,  
1290 vol. 397–399, no. March 2021, pp. 103–112, 2022, doi: 10.1016/j.cattod.2021.11.022.
- 1291 [66] M. Feyen *et al.*, “High-temperature stable, iron-based core-shell catalysts for ammonia  
1292 decomposition,” *Chem. - A Eur. J.*, vol. 17, no. 2, pp. 598–605, 2011, doi:  
1293 10.1002/chem.201001827.
- 1294 [67] H. Zhang *et al.*, “Tuning catalytic performances of cobalt catalysts for clean hydrogen  
1295 generation via variation of the type of carbon support and catalyst post-treatment  
1296 temperature,” *Int. J. Hydrogen Energy*, vol. 39, no. 31, pp. 17573–17582, 2014, doi:  
1297 10.1016/j.ijhydene.2014.07.183.
- 1298 [68] T. A. Le *et al.*, “Ru-supported lanthania-ceria composite as an efficient catalyst for  
1299 CO<sub>x</sub>-free H<sub>2</sub> production from ammonia decomposition,” *Appl. Catal. B Environ.*, vol.  
1300 285, no. September 2020, p. 119831, 2021, doi: 10.1016/j.apcatb.2020.119831.

- 1301 [69] Z. W. Wu, X. Li, Y. H. Qin, L. Deng, C. W. Wang, and X. Jiang, “Ammonia  
1302 decomposition over SiO<sub>2</sub>-supported Ni–Co bimetallic catalyst for CO<sub>x</sub>-free hydrogen  
1303 generation,” *Int. J. Hydrogen Energy*, vol. 45, no. 30, pp. 15263–15269, 2020, doi:  
1304 10.1016/j.ijhydene.2020.04.007.
- 1305 [70] S. Podila, Y. A. Alhamed, A. A. Alzahrani, and L. A. Petrov, “Hydrogen production  
1306 by ammonia decomposition using Co catalyst supported on Mg mixed oxide systems,”  
1307 *Int. J. Hydrogen Energy*, vol. 40, no. 45, pp. 15411–15422, 2015, doi:  
1308 10.1016/j.ijhydene.2015.09.057.
- 1309 [71] M. Pinzón, A. Romero, A. de Lucas-Consuegra, A. R. de la Osa, and P. Sánchez,  
1310 “CO<sub>x</sub>-free hydrogen production from ammonia at low temperature using Co/SiC  
1311 catalyst: Effect of promoter,” *Catal. Today*, vol. 390–391, no. November 2021, pp. 34–  
1312 47, 2022, doi: 10.1016/j.cattod.2021.12.005.
- 1313 [72] Y. Sakata, Y. Tamaura, H. Imamura, and M. Watanabe, “Preparation of a new type of  
1314 CaSiO<sub>3</sub> with high surface area and property as a catalyst support,” *Stud. Surf. Sci.*  
1315 *Catal.*, vol. 162, pp. 331–338, 2006, doi: 10.1016/S0167-2991(06)80924-9.
- 1316 [73] S. Mazzone, T. Goklany, G. Zhang, J. Tan, E. I. Papaioannou, and F. R. García-García,  
1317 “Ruthenium-based catalysts supported on carbon xerogels for hydrogen production via  
1318 ammonia decomposition,” *Appl. Catal. A Gen.*, vol. 632, no. January, p. 118484, 2022,  
1319 doi: 10.1016/j.apcata.2022.118484.
- 1320 [74] M. El-Shafie, S. Kambara, and Y. Hayakawa, “Alumina particle size effect on H<sub>2</sub>  
1321 production from ammonia decomposition by DBD plasma,” *Energy Reports*, vol. 6,  
1322 pp. 25–30, 2020, doi: 10.1016/j.egy.2020.10.032.
- 1323 [75] Ł. Czekajło and Z. Lendzion-Bieluń, “Effect of preparation conditions and promoters  
1324 on the structure and activity of the ammonia decomposition reaction catalyst based on  
1325 nanocrystalline cobalt,” *Chem. Eng. J.*, vol. 289, pp. 254–260, 2016, doi:  
1326 10.1016/j.cej.2015.12.093.
- 1327 [76] L. Li, S. Wang, Z. Zhu, X. Yao, and Z. Yan, “Catalytic decomposition of ammonia  
1328 over fly ash supported Ru catalysts,” *Fuel Process. Technol.*, vol. 89, no. 11, pp.  
1329 1106–1112, 2008, doi: 10.1016/j.fuproc.2008.05.002.
- 1330 [77] Z. Lendzion-Bielun, U. Narkiewicz, and W. Arabczyk, “Cobalt-based catalysts for



- 1331 ammonia decomposition,” *Materials (Basel)*., vol. 6, no. 6, pp. 2400–2409, 2013, doi:  
1332 10.3390/ma6062400.
- 1333 [78] Y. Li *et al.*, “Size structure-catalytic performance correlation of supported Ni/MCF-17  
1334 catalysts for CO: X-free hydrogen production,” *Chem. Commun.*, vol. 54, no. 49, pp.  
1335 6364–6367, 2018, doi: 10.1039/c8cc01884g.
- 1336 [79] C. Huang *et al.*, “Hydrogen generation by ammonia decomposition over Co/CeO<sub>2</sub>  
1337 catalyst: Influence of support morphologies,” *Appl. Surf. Sci.*, vol. 532, no. July, 2020,  
1338 doi: 10.1016/j.apsusc.2020.147335.
- 1339 [80] H. Kominami, H. Nishimune, Y. Ohta, Y. Arakawa, and T. Inaba, “Photocatalytic  
1340 hydrogen formation from ammonia and methyl amine in an aqueous suspension of  
1341 metal-loaded titanium(IV) oxide particles,” *Appl. Catal. B Environ.*, vol. 111–112, pp.  
1342 297–302, 2012, doi: 10.1016/j.apcatb.2011.10.011.
- 1343 [81] K. Obata, K. Kishishita, A. Okemoto, K. Taniya, Y. Ichihashi, and S. Nishiyama,  
1344 “Photocatalytic decomposition of NH<sub>3</sub> over TiO<sub>2</sub> catalysts doped with Fe,” *Appl.*  
1345 *Catal. B Environ.*, vol. 160–161, no. 1, pp. 200–203, 2014, doi:  
1346 10.1016/j.apcatb.2014.05.033.
- 1347 [82] M. Reli *et al.*, “Novel cerium doped titania catalysts for photocatalytic decomposition  
1348 of ammonia,” *Appl. Catal. B Environ.*, vol. 178, pp. 108–116, 2015, doi:  
1349 10.1016/j.apcatb.2014.10.021.
- 1350 [83] A. Iwase, K. Ii, and A. Kudo, “Decomposition of an aqueous ammonia solution as a  
1351 photon energy conversion reaction using a Ru-loaded ZnS photocatalyst,” *Chem.*  
1352 *Commun.*, vol. 54, no. 48, pp. 6117–6119, Jun. 2018, doi: 10.1039/C8CC02639D.
- 1353 [84] S. Abdul Razak, A. H. Mahadi, R. Thotagamuge, D. Prasetyoko, and H. Bahruji,  
1354 “Photocatalytic Hydrogen Gas Production from NH<sub>3</sub> and Alkylamine: Route to Zero  
1355 Carbon Emission Energy,” *Catal. Letters*, no. 0123456789, 2022, doi:  
1356 10.1007/s10562-022-04049-5.
- 1357 [85] W. Xu *et al.*, “Electrodeposited NiCu bimetal on carbon paper as stable non-noble  
1358 anode for efficient electrooxidation of ammonia,” *Appl. Catal. B Environ.*, vol. 237,  
1359 pp. 1101–1109, 2018, doi: 10.1016/j.apcatb.2016.11.003.
- 1360 [86] A. Allagui, S. Sarfraz, S. Ntais, F. Al Momani, and E. A. Baranova, “Electrochemical

- 1361 behavior of ammonia on Ni<sub>98</sub>Pd<sub>2</sub> nano-structured catalyst,” *Int. J. Hydrogen Energy*,  
1362 vol. 39, no. 1, pp. 41–48, 2014, doi: 10.1016/j.ijhydene.2013.10.024.
- 1363 [87] N. M. Adli, H. Zhang, S. Mukherjee, and G. Wu, “Review—Ammonia Oxidation  
1364 Electrocatalysis for Hydrogen Generation and Fuel Cells,” *J. Electrochem. Soc.*, vol.  
1365 165, no. 15, pp. J3130–J3147, 2018, doi: 10.1149/2.0191815jes.
- 1366 [88] K. Jiang *et al.*, “Nickel-cobalt nitride nanoneedle supported on nickel foam as an  
1367 efficient electrocatalyst for hydrogen generation from ammonia electrolysis,”  
1368 *Electrochim. Acta*, vol. 403, p. 139700, 2022, doi: 10.1016/j.electacta.2021.139700.
- 1369 [89] Z. Zhang, S. Zhang, Q. Yao, X. Chen, and Z. H. Lu, “Controlled Synthesis of MOF-  
1370 Encapsulated NiPt Nanoparticles toward Efficient and Complete Hydrogen Evolution  
1371 from Hydrazine Borane and Hydrazine,” *Inorg. Chem.*, vol. 56, no. 19, pp. 11938–  
1372 11945, 2017, doi: 10.1021/acs.inorgchem.7b01910.
- 1373 [90] D. Bhattacharjee, K. Mandal, and S. Dasgupta, “High performance nickel-palladium  
1374 nanocatalyst for hydrogen generation from alkaline hydrous hydrazine at room  
1375 temperature,” *J. Power Sources*, vol. 287, pp. 96–99, 2015, doi:  
1376 10.1016/j.jpowsour.2015.04.008.
- 1377 [91] S. K. Singh, Z. H. Lu, and Q. Xu, “Temperature-induced enhancement of catalytic  
1378 performance in selective hydrogen generation from hydrous hydrazine with Ni-based  
1379 nanocatalysts for chemical hydrogen storage,” *Eur. J. Inorg. Chem.*, no. 14, pp. 2232–  
1380 2237, 2011, doi: 10.1002/ejic.201100083.
- 1381 [92] H. Zou, Q. Yao, M. Huang, M. Zhu, F. Zhang, and Z. H. Lu, “Noble-metal-free NiFe  
1382 nanoparticles immobilized on nano CeZrO<sub>2</sub> solid solutions for highly efficient  
1383 hydrogen production from hydrous hydrazine,” *Sustain. Energy Fuels*, vol. 3, no. 11,  
1384 pp. 3071–3077, 2019, doi: 10.1039/c9se00547a.
- 1385 [93] X. Liu, Y. Liu, J. Wang, and J. Ma, “Anatase-Type TiO<sub>2</sub>-Modified Amorphous NiMo  
1386 Nanoparticles with Superior Catalytic Performance toward Dehydrogenation of  
1387 Hydrous Hydrazine,” *Ind. Eng. Chem. Res.*, vol. 61, no. 4, pp. 1636–1643, 2022, doi:  
1388 10.1021/acs.iecr.1c03398.
- 1389 [94] K. S. Al-Thubaiti and Z. Khan, “Trimetallic nanocatalysts to enhanced hydrogen  
1390 production from hydrous hydrazine: The role of metal centers,” *Int. J. Hydrogen*

- 1391 *Energy*, vol. 45, no. 27, pp. 13960–13974, 2020, doi: 10.1016/j.ijhydene.2020.03.093.
- 1392 [95] S. K. Singh, X. B. Zhang, and Q. Xu, “Room-temperature hydrogen generation from  
1393 hydrous hydrazine for chemical hydrogen storage,” *J. Am. Chem. Soc.*, vol. 131, no.  
1394 29, pp. 9894–9895, 2009, doi: 10.1021/ja903869y.
- 1395 [96] D. Motta, I. Barlocco, S. Bellomi, A. Villa, and N. Dimitratos, “Hydrous hydrazine  
1396 decomposition for hydrogen production using of ir/ceo2: Effect of reaction parameters  
1397 on the activity,” *Nanomaterials*, vol. 11, no. 5, pp. 1–15, 2021, doi:  
1398 10.3390/nano11051340.
- 1399 [97] W. Kang and A. Varma, “Hydrogen generation from hydrous hydrazine over Ni/CeO2  
1400 catalysts prepared by solution combustion synthesis,” *Appl. Catal. B Environ.*, vol.  
1401 220, no. April 2017, pp. 409–416, 2018, doi: 10.1016/j.apcatb.2017.08.053.
- 1402 [98] S. K. Singh, Y. Iizuka, and Q. Xu, “Nickel-palladium nanoparticle catalyzed hydrogen  
1403 generation from hydrous hydrazine for chemical hydrogen storage,” *Int. J. Hydrogen  
1404 Energy*, vol. 36, no. 18, pp. 11794–11801, 2011, doi: 10.1016/j.ijhydene.2011.06.069.
- 1405 [99] L. He *et al.*, “A Noble-Metal-Free Catalyst Derived from Ni-Al Hydrotalcite for  
1406 Hydrogen Generation from N<sub>2</sub>H<sub>4</sub>·H<sub>2</sub>O Decomposition,” *Angew. Chemie*, vol. 124, no.  
1407 25, pp. 6295–6298, 2012, doi: 10.1002/ange.201201737.
- 1408 [100] O. Song-Il, J. M. Yan, H. L. Wang, Z. L. Wang, and Q. Jiang, “High catalytic kinetic  
1409 performance of amorphous CoPt NPs induced on CeO<sub>x</sub> for H<sub>2</sub> generation from  
1410 hydrous hydrazine,” *Int. J. Hydrogen Energy*, vol. 39, no. 8, pp. 3755–3761, 2014, doi:  
1411 10.1016/j.ijhydene.2013.12.135.
- 1412 [101] Z. Zhang, Z.-H. Lu, H. Tan, X. Chen, and Q. Yao, “CeO<sub>x</sub>-modified RhNi  
1413 nanoparticles grown on rGO as highly efficient catalysts for complete hydrogen  
1414 generation from hydrazine borane and hydrazine †,” *J. Mater. Chem. A*, vol. 3, pp.  
1415 23520–23529, 2015, doi: 10.1039/c5ta06197k.
- 1416 [102] P. Zhao, N. Cao, W. Luo, and G. Cheng, “Nanoscale MIL-101 supported RhNi  
1417 nanoparticles: An efficient catalyst for hydrogen generation from hydrous hydrazine,”  
1418 *J. Mater. Chem. A*, vol. 3, no. 23, pp. 12468–12475, 2015, doi: 10.1039/c5ta02201k.
- 1419 [103] B. Xia, K. Chen, W. Luo, and G. Cheng, “NiRh nanoparticles supported on nitrogen-  
1420 doped porous carbon as highly efficient catalysts for dehydrogenation of hydrazine in

- 1421 alkaline solution,” *Nano Res.*, vol. 8, no. 11, pp. 3472–3479, 2015, doi:  
1422 10.1007/s12274-015-0845-4.
- 1423 [104] H. Dai, Y. Zhong, and P. Wang, “Hydrogen generation from decomposition of hydrous  
1424 hydrazine over Ni-Ir/CeO<sub>2</sub> catalyst,” *Prog. Nat. Sci. Mater. Int.*, vol. 27, no. 1, pp.  
1425 121–125, 2017, doi: 10.1016/j.pnsc.2016.12.012.
- 1426 [105] H. Wang *et al.*, “Ni nanoparticles encapsulated in the channel of titanate nanotubes : E  
1427 ffi cient noble-metal-free catalysts for selective hydrogen generation from hydrous  
1428 hydrazine,” *Chem. Eng. J.*, vol. 332, no. July 2017, pp. 637–646, 2018, doi:  
1429 10.1016/j.cej.2017.09.126.
- 1430 [106] Q. Yao, M. He, X. Hong, X. Chen, G. Feng, and Z. H. Lu, “Hydrogen production via  
1431 selective dehydrogenation of hydrazine borane and hydrous hydrazine over MoO<sub>x</sub>-  
1432 promoted Rh catalyst,” *Int. J. Hydrogen Energy*, vol. 44, no. 53, pp. 28430–28440,  
1433 2019, doi: 10.1016/j.ijhydene.2019.02.105.
- 1434 [107] Y. P. Qiu, H. Yin, H. Dai, L. Y. Gan, H. Bin Dai, and P. Wang, “Tuning the Surface  
1435 Composition of Ni/meso-CeO<sub>2</sub> with Iridium as an Efficient Catalyst for Hydrogen  
1436 Generation from Hydrous Hydrazine,” *Chem. - A Eur. J.*, vol. 24, no. 19, pp. 4902–  
1437 4908, 2018, doi: 10.1002/chem.201705923.
- 1438 [108] Q. Shi, Y. P. Qiu, H. Dai, and P. Wang, “Study of formation mechanism of Ni-  
1439 Pt/CeO<sub>2</sub> catalyst for hydrogen generation from hydrous hydrazine,” *J. Alloys Compd.*,  
1440 vol. 787, pp. 1187–1194, 2019, doi: 10.1016/j.jallcom.2019.01.378.
- 1441 [109] Q. Shi *et al.*, “Noble-Metal-Free Ni-W-O-Derived Catalysts for High-Capacity  
1442 Hydrogen Production from Hydrazine Monohydrate,” *ACS Sustain. Chem. Eng.*, vol.  
1443 8, no. 14, pp. 5595–5603, 2020, doi: 10.1021/acssuschemeng.9b07782.
- 1444 [110] Y. J. Zhong *et al.*, “Highly efficient Ni@Ni-Pt/La<sub>2</sub>O<sub>3</sub> catalyst for hydrogen generation  
1445 from hydrous hydrazine decomposition: Effect of Ni-Pt surface alloying,” *J. Power  
1446 Sources*, vol. 300, pp. 294–300, 2015, doi: 10.1016/j.jpowsour.2015.09.071.
- 1447 [111] L. He *et al.*, “Structural and catalytic properties of supported Ni-Ir alloy catalysts for  
1448 H<sub>2</sub> generation via hydrous hydrazine decomposition,” *Appl. Catal. B Environ.*, vol.  
1449 147, pp. 779–788, 2014, doi: 10.1016/j.apcatb.2013.10.022.
- 1450 [112] S. K. Singh, A. K. Singh, K. Aranishi, and Q. Xu, “Noble-Metal-Free Bimetallic

- 1451 Nanoparticle-Catalyzed Selective,” pp. 19638–19641, 2011.
- 1452 [113] H. Wang, L. Wu, Y. Wang, X. Li, and Y. Wang, “Facile synthesis of Ni nanoparticles  
1453 from triangular Ni(HCO<sub>3</sub>)<sub>2</sub> nanosheets as catalysts for hydrogen generation from  
1454 hydrous hydrazine,” *Catal. Commun.*, vol. 100, no. March, pp. 33–37, 2017, doi:  
1455 10.1016/j.catcom.2017.06.021.
- 1456 [114] Q. Yao *et al.*, “Alkali-assisted synthesis of ultrafine NiPt nanoparticles immobilized on  
1457 La<sub>2</sub>O<sub>2</sub>CO<sub>3</sub> for highly efficient dehydrogenation of hydrous hydrazine and hydrazine  
1458 borane,” *Catal. Today*, vol. 400–401, no. June 2021, pp. 49–58, 2022, doi:  
1459 10.1016/j.cattod.2021.11.023.
- 1460 [115] W. Huang and X. Liu, “The ‘on–off’ switch for on-demand H<sub>2</sub> evolution from hydrous  
1461 hydrazine over Ni<sub>8</sub>Pt<sub>1</sub>/C nano-catalyst,” *Fuel*, vol. 315, no. January, p. 123210, 2022,  
1462 doi: 10.1016/j.fuel.2022.123210.
- 1463 [116] M. Hinojosa-Reyes, A. Hernández-Gordillo, R. Zanella, and V. Rodríguez-González,  
1464 “Renewable hydrogen harvest process by hydrazine as scavenging electron donor  
1465 using gold TiO<sub>2</sub> photocatalysts,” *Catal. Today*, vol. 266, pp. 2–8, 2016, doi:  
1466 10.1016/j.cattod.2015.10.002.
- 1467 [117] A. E. Raevskaya *et al.*, “Photocatalytic H<sub>2</sub> production from aqueous solutions of  
1468 hydrazine and its derivatives in the presence of nitric-acid-activated graphitic carbon  
1469 nitride,” *Catal. Today*, vol. 284, pp. 229–235, 2017, doi: 10.1016/j.cattod.2016.12.024.
- 1470 [118] P. Kumar *et al.*, “Visible light assisted hydrogen generation from complete  
1471 decomposition of hydrous hydrazine using rhodium modified TiO<sub>2</sub> photocatalysts,”  
1472 *Photochem. Photobiol. Sci.*, vol. 16, no. 7, pp. 1036–1042, 2017, doi:  
1473 10.1039/c6pp00432f.
- 1474 [119] J. Sanabria-Chinchilla, K. Asazawa, T. Sakamoto, K. Yamada, H. Tanaka, and P.  
1475 Strasser, “Noble metal-free hydrazine fuel cell catalysts: EPOC effect in competing  
1476 chemical and electrochemical reaction pathways,” *J. Am. Chem. Soc.*, vol. 133, no. 14,  
1477 pp. 5425–5431, 2011, doi: 10.1021/ja111160r.
- 1478 [120] T. Y. Jeon, M. Watanabe, and K. Miyatake, “Carbon segregation-induced highly  
1479 metallic Ni nanoparticles for electrocatalytic oxidation of hydrazine in alkaline  
1480 media,” *ACS Appl. Mater. Interfaces*, vol. 6, no. 21, pp. 18445–18449, 2014, doi:

- 1481 10.1021/am5058635.
- 1482 [121] S. S. Narwade, B. B. Mulik, S. M. Mali, and B. R. Sathe, “Silver nanoparticles  
1483 sensitized C 60 (Ag@C 60 ) as efficient electrocatalysts for hydrazine oxidation:  
1484 Implication for hydrogen generation reaction,” *Appl. Surf. Sci.*, vol. 396, pp. 939–944,  
1485 2017, doi: 10.1016/j.apsusc.2016.11.065.
- 1486 [122] X. Yan, Y. Chen, M. Yang, Y. Shi, T. Gao, and Y. Li, “Efficient and Long-term  
1487 Photoelectrochemical Hydrogen Liberation from Hydrazine Hydrate on CdS Nanorod  
1488 Arrays,” *J. Electron. Mater.*, vol. 51, no. 6, pp. 3114–3124, 2022, doi:  
1489 10.1007/s11664-022-09559-x.
- 1490 [123] N. Morlanés *et al.*, “A technological roadmap to the ammonia energy economy:  
1491 Current state and missing technologies,” *Chem. Eng. J.*, vol. 408, no. August 2020,  
1492 2021, doi: 10.1016/j.cej.2020.127310.
- 1493 [124] A. Di Carlo, A. Dell’Era, and Z. Del Prete, “3D simulation of hydrogen production by  
1494 ammonia decomposition in a catalytic membrane reactor,” *Int. J. Hydrogen Energy*,  
1495 vol. 36, no. 18, pp. 11815–11824, 2011, doi: 10.1016/j.ijhydene.2011.06.029.
- 1496 [125] N. Itoh, Y. Kikuchi, T. Furusawa, and T. Sato, “Tube-wall catalytic membrane reactor  
1497 for hydrogen production by low-temperature ammonia decomposition,” *Int. J.*  
1498 *Hydrogen Energy*, vol. 46, no. 38, pp. 20257–20265, 2021, doi:  
1499 10.1016/j.ijhydene.2020.03.162.
- 1500 [126] M. E. E. Abashar, “Multi-stage membrane reactors for hydrogen production by  
1501 ammonia decomposition,” *Int. J. Petrochemistry Res.*, vol. 2, no. 1, pp. 109–115, 2018,  
1502 doi: 10.18689/ijpr-1000120.
- 1503 [127] J. L. Cerrillo *et al.*, “High purity, self-sustained, pressurized hydrogen production from  
1504 ammonia in a catalytic membrane reactor,” *Chem. Eng. J.*, vol. 431, no. December  
1505 2021, 2022, doi: 10.1016/j.cej.2021.134310.
- 1506 [128] V. Cechetto, L. Di Felice, R. Gutierrez Martinez, A. Arratibel Plazaola, and F.  
1507 Gallucci, “Ultra-pure hydrogen production via ammonia decomposition in a catalytic  
1508 membrane reactor,” *Int. J. Hydrogen Energy*, vol. 47, no. 49, pp. 21220–21230, 2022,  
1509 doi: 10.1016/j.ijhydene.2022.04.240.
- 1510 [129] S. Shwe Hla and M. D. Dolan, “CFD modelling of a membrane reactor for hydrogen

- 1511 production from ammonia,” *IOP Conf. Ser. Mater. Sci. Eng.*, vol. 297, no. 1, 2018,  
1512 doi: 10.1088/1757-899X/297/1/012027.
- 1513 [130] H. Cheng *et al.*, “Single-step synthesized dual-layer hollow fiber membrane reactor for  
1514 on-site hydrogen production through ammonia decomposition,” *Int. J. Hydrogen*  
1515 *Energy*, vol. 45, no. 12, pp. 7423–7432, 2020, doi: 10.1016/j.ijhydene.2019.04.101.
- 1516 [131] Z. Zhang, S. Liguori, T. F. Fuerst, J. D. Way, and C. A. Wolden, “Efficient Ammonia  
1517 Decomposition in a Catalytic Membrane Reactor to Enable Hydrogen Storage and  
1518 Utilization,” *ACS Sustain. Chem. Eng.*, vol. 7, no. 6, pp. 5975–5985, 2019, doi:  
1519 10.1021/acssuschemeng.8b06065.
- 1520 [132] S. Chiuta, R. C. Everson, H. W. J. P. Neomagus, P. Van Der Gryp, and D. G.  
1521 Bessarabov, “Reactor technology options for distributed hydrogen generation via  
1522 ammonia decomposition: A review,” *Int. J. Hydrogen Energy*, vol. 38, no. 35, pp.  
1523 14968–14991, 2013, doi: 10.1016/j.ijhydene.2013.09.067.
- 1524 [133] Y. L. Chen, C. F. Juang, and Y. C. Chen, “The effects of promoter cs loading on the  
1525 hydrogen production from ammonia decomposition using ru/c catalyst in a fixed-bed  
1526 reactor,” *Catalysts*, vol. 11, no. 3, pp. 1–15, 2021, doi: 10.3390/catal11030321.
- 1527 [134] Y. Gu, Y. Ma, Z. Long, S. Zhao, Y. Wang, and W. Zhang, “One-pot synthesis of  
1528 supported Ni@Al<sub>2</sub>O<sub>3</sub> catalysts with uniform small-sized Ni for hydrogen generation  
1529 via ammonia decomposition,” *Int. J. Hydrogen Energy*, vol. 46, no. 5, pp. 4045–4054,  
1530 2021, doi: 10.1016/j.ijhydene.2020.11.003.
- 1531 [135] N. Morlanés *et al.*, “Development of a Ba-CoCe catalyst for the efficient and stable  
1532 decomposition of ammonia,” *Catal. Sci. Technol.*, vol. 11, no. 9, pp. 3014–3024, 2021,  
1533 doi: 10.1039/d0cy02336a.
- 1534 [136] F. Zhiqiang *et al.*, “Catalytic ammonia decomposition to CO<sub>x</sub>-free hydrogen over  
1535 ruthenium catalyst supported on alkali silicates,” *Fuel*, vol. 326, no. April, p. 125094,  
1536 2022, doi: 10.1016/j.fuel.2022.125094.
- 1537 [137] I. Lucentini, G. García Colli, C. D. Luzi, I. Serrano, O. M. Martínez, and J. Llorca,  
1538 “Catalytic ammonia decomposition over Ni-Ru supported on CeO<sub>2</sub> for hydrogen  
1539 production: Effect of metal loading and kinetic analysis,” *Appl. Catal. B Environ.*, vol.  
1540 286, no. December 2020, 2021, doi: 10.1016/j.apcatb.2021.119896.

- 1541 [138] I. Lucentini *et al.*, “Modelling and simulation of catalytic ammonia decomposition  
1542 over Ni-Ru deposited on 3D-printed CeO<sub>2</sub>,” *Chem. Eng. J.*, vol. 427, no. July 2021,  
1543 2022, doi: 10.1016/j.cej.2021.131756.
- 1544 [139] L. A. Jolaoso *et al.*, “Ammonia decomposition over citric acid induced  $\gamma$ -Mo<sub>2</sub>N and  
1545 Co<sub>3</sub>Mo<sub>3</sub>N catalysts,” *Int. J. Hydrogen Energy*, vol. 43, no. 10, pp. 4839–4844, 2018,  
1546 doi: 10.1016/j.ijhydene.2018.01.092.
- 1547 [140] A. R. Kim *et al.*, “Hydrogen production from ammonia decomposition over Ru-rich  
1548 surface on La<sub>2</sub>O<sub>2</sub>CO<sub>3</sub>-Al<sub>2</sub>O<sub>3</sub> catalyst beads,” *Catal. Today*, no. April, 2022, doi:  
1549 10.1016/j.cattod.2022.08.009.
- 1550 [141] X. Vendrell, J. Llorca, and I. Lucentini, “Review of the Decomposition of Ammonia to  
1551 Generate Hydrogen,” 2021, doi: 10.1021/acs.iecr.1c00843.
- 1552 [142] N. Engelbrecht, S. Chiuta, and D. G. Bessarabov, “A highly efficient autothermal  
1553 microchannel reactor for ammonia decomposition: Analysis of hydrogen production in  
1554 transient and steady-state regimes,” *J. Power Sources*, vol. 386, no. February, pp. 47–  
1555 55, 2018, doi: 10.1016/j.jpowsour.2018.03.043.
- 1556 [143] K. Schumacher, N. Engelbrecht, R. C. Everson, M. Friedl, and D. G. Bessarabov,  
1557 “Steady-state and transient modelling of a microchannel reactor for coupled ammonia  
1558 decomposition and oxidation,” *Int. J. Hydrogen Energy*, vol. 44, no. 13, pp. 6415–  
1559 6426, 2019, doi: 10.1016/j.ijhydene.2019.01.132.
- 1560 [144] K. Gyak, N. K. Vishwakarma, Y. Hwang, J. Kim, H. Yun, and D. Kim, “Reaction  
1561 Chemistry & Engineering from a photocurable preceramic resin for the high  
1562 temperature ammonia cracking process †,” pp. 1393–1399, 2019, doi:  
1563 10.1039/c9re00201d.
- 1564 [145] H. Maleki, M. Fulton, and V. Bertola, “Kinetic assessment of H<sub>2</sub> production from  
1565 NH<sub>3</sub> decomposition over CoCeAlO catalyst in a microreactor: Experiments and CFD  
1566 modelling,” *Chem. Eng. J.*, vol. 411, no. December 2020, p. 128595, 2021, doi:  
1567 10.1016/j.cej.2021.128595.
- 1568 [146] C. Chen *et al.*, “Bimetallic Ru-Fe Nanoparticles Supported on Carbon Nanotubes for  
1569 Ammonia Decomposition and Synthesis,” *Chem. Eng. Technol.*, vol. 43, no. 4, pp.  
1570 719–730, 2020, doi: 10.1002/ceat.201900508.



